Applied Energy 186 (2017) 262–281

Contents lists available at ScienceDirect

Applied Energy

journal homepage: www.elsevier.com/locate/apenergy

Dynamic modelling and experimental validation of scroll expander for small scale power generation system

Zhiwei Ma, Huashan Bao *, Anthony Paul Roskilly

Sir Joseph Swan Centre for Energy Research, Newcastle University, Newcastle upon Tyne NE1 7RU, UK

HIGHLIGHTS

- A detailed and generic dynamic modelling and simulation method of scroll expander.
- An overall dynamic friction coefficient was proposed to enhance the adaptability.
- The present method has been validated by several sets of experimental results.
- The overall dynamic friction coefficient was found at the magnitude of 10^{-3} N m s.

ARTICLE INFO

Article history:
Received 19 March 2016
Received in revised form 2 August 2016
Accepted 4 August 2016
Available online 17 August 2016

Keywords:
Scroll expander
Modelling and simulation
Experimental validation
Overall dynamic friction coefficient
Power generation

ABSTRACT

This work presents a detailed and generic dynamic modelling and simulation method of scroll expander for small scale power generation system. The geometric models of the scroll were built step by step, including the scroll involute, scroll dimensions, chamber areas and volumes, the scroll profile modifications and so on. The valve model, internal leakage model, motion equation, heat transfer equation and energy balance equation were combined with the geometric models to complete the scroll expander modelling. A mathematic model of a direct current generator or an experimentally determined correlation of generated power against rotational speed of the used generator was integrated to the expander model as the power output unit. To enhance the adaptability of the current model, an overall dynamic friction coefficient of the scroll expander and the generator was innovatively proposed and introduced as one of the key parameters in the present study. The accurate value of this coefficient should be experimentally determined for a specific expander – generator system; with the knowledge of such a parameter, the mechanical friction loss can be accurately and easily calculated in the simulation study. The present modelling and simulation method have been validated by several sets of experimental results based on different scroll expanders studied by different researchers, and the corresponding overall dynamic friction coefficient was found in the order of magnitude of 10^{-3} N m s.

1. Introduction

A great number of research efforts have been made to effectively utilise the ubiquitous renewable energy sources, such as solar energy, wind energy and geothermal energy as well as enormous amount of industrial waste heat, directly or convert them to electricity. Various thermodynamic cycles have been proposed and studied to recover low grade heat for electricity generation, such as organic Rankine cycle (ORC), Kalina cycle and trilateral flash cycle. Turbine/expander is one of the key components in these power generation systems, the selection of which is critical to the system energy efficiency and cost effectiveness. As a positive displacement type expander, orbiting scroll expander has attracted many interests in the application of small scale power generation system [1–3]. Although the scroll expander has complicated geometric design and manufacture, and the fixed build-in volume ratio limits the expansion ratio and therefore limits its application, it presents as a good choice for small scale power generation system within the capacity range of 0.1–10 kW, with following advantages [1–3]:

- High isentropic efficiency.
- Mechanical simplicity, e.g. no valves and gears.
- Less moving parts.
- Low rotational speed.
- Low noise and vibration.
- High reliability and robustness.

* Corresponding author.
E-mail address: huashan.bao@newcastle.ac.uk (H. Bao).

http://dx.doi.org/10.1016/j.apenergy.2016.08.025
0306-2619/

Nomenclature

a	basic circle radius (m)
A	area (m^2)
A_{max}	oscillating amplitude (m)
B	viscous friction coefficient (N m s)
c_p, c_v	heat capacity (J kg^{-1} K^{-1})
C_V	valve capacity coefficient (–)
D_c	diameter of scroll curvature (m)
D_h	hydraulic diameter (m)
E_a	back electromotive force (V)
f_r, f_f	flow coefficient (–)
f_o	oscillating frequency (s^{-1})
f_{SG}	overall dynamic friction coefficient of scroll and generator (N m s)
F	force (N)
F_P	piping geometry factor (–)
h_s	scroll height (m)
h	enthalpy (J kg^{-1})
I_a	current (A)
J	moment of inertia (kg m^2)
K_e	constant of back electromotive force (V s rad^{-1})
K_t	torque constant (N m A^{-1})
l	length (m)
L_a	armature inductance (H)
L_r, L_f	leakage length (m)
m	mass (kg)
$\dot{m}$	mass flow rate (kg s^{-1})
N_C	expansion chamber number (–)
Nu	Nusselt number (–)
N_6	constant in valve model (–)
P	pressure (Pa)
Pit	scroll pitch (m)
Pr	Prandtl number (–)
Q	heat (J)
$\dot{Q}$	heat transfer rate (W)
R	resistance (Ω)
Re	Reynolds number (–)
R_{sh}	shell radius (m)
R_{or}	orbiting radius (m)
S	area (m^2)
St	Strouhal number (–)
t	time (s)
t_{Plate}	base plate thickness (m)
t_s	scroll thickness (m)
u	internal energy (J kg^{-1})
$\overline{U}$	mean flow velocity (m s^{-1})
V	volume (m^3)
$\dot{W}$	rate of work output (W)
x, y	coordinate (m)
x_P	pressure drop ratio (–)
x_T	critical pressure drop ratio (–)
Y	expansion factor (–)

Greek letters

α	initial involute angle (rad)
α_{amb}	ambient heat transfer coefficient (W m^2 K^{-1})
β, γ, λ	angles used in scroll modification (rad)
δ_r, δ_f	leakage clearance size (m)
ε	expansion ratio (–)
η	efficiency (–)
θ	orbiting angle (rad)
λ	thermal conductivity (W m^{-1} K^{-1})
ρ	radius of involute (m)
ϕ	involute angle (rad)
ϕ_P	involute angle of cutter point (rad)
ω	angular velocity (rad s^{-1})

Subscripts

a	axial
amb	ambient
arm	armature
b	back
C	chamber
C*i*	chamber *i*
DB	Dittus-Boelter
d	downstream
disc	disconnection
e	end
em	electromechanical
f	fixed scroll / flank
fr	friction
i	inner
in	inlet
mc	modification by cutter
mp	modification by PMP
o	outer / orbiting scroll
orb	orbiting
out	outlet
Old	Oldham ring
u	upstream
r	radial
sha	shaft
t	tangent
WF	working fluid

Experimental and numerical researches on the application of scroll expander in ORC system have been extensively reported in recent years. Thanks to the broad development and utilisation of scroll type compressor in refrigeration, air conditioning and heat pump area, a scroll machinery is readily available and only requires little effort to be converted to a scroll type expander. Lemort et al. [4] modified a hermetic scroll compressor used in a heat pump system to an expander for an ORC system using HFC-245fa as working fluid. The isentropic efficiency of the expander could reach 71.03% but it was found reducing with oil quantity. Bracco et al. [5] built a 1.5 kW domestic scale ORC system which had a retrofitted hermetic scroll expander and used HFC-245fa as working fluid, the corresponding expander isentropic efficiency and thermal efficiency were in the range of 57–75% and 7.1–8.6% respectively when the evaporation temperature was not higher than 150 °C. Compared to hermetic scroll compressor, retrofitting an open-drive scroll air compressor to expander seems to be more straightforward. Lemort et al. [6] and Quoilin et al. [7] tested and modelled a scroll expander which was retrofitted from an open-drive oil-free air scroll compressor, and obtained the maximum isentropic efficiency 68% when using R123 as the working fluid. The numerical study quantified the energy losses and suggested that the internal leakage, supply pressure drop and mechanical loss were the three major losses that deteriorated the scroll expander performance. The authors reported based on the simulation results that the maximum system thermal efficiency was 9.9% by adjusting the rotational speed of the expander. Both Declaye et al. [8] and Chen et al. [9] adapted an open-drive oil-free scroll type air compressor to expander and applied them to an ORC systems with HFC-245fa as working fluid. The former tests achieved a maximum thermal efficiency at 8.5% and maximum expander isentropic efficiency at 75.7% when the evaporation and condensation temperatures at

97.5 °C and 26.6 °C, respectively; while the latter research obtained similar results as these two maximum efficiencies were 9.44% and 73.1% respectively when evaporation temperature lower than 100 °C. Chen et al. [9] also pointed out the noteworthy efficiency improvement by using larger superheating degree. Other than the laboratory modification, a few commercially designed and manufactured scroll expander has emerged as well, for example, Galloni et al. [10] applied a scroll expander developed by Air Squared Inc.© to a mini-ORC system with HFC-245fa as working fluid. With evaporation temperature lower than 100 °C, the obtained maximum thermal efficiency was 9.28% while the expander isentropic efficiency was 84.9%. More researches about employing scroll expanders in ORC systems can be found in literature [3].

Scroll expander has also been used in other power generation systems. Mendoza et al. [11] tested the performance of a scroll expander using ammonia as working fluid, and concluded that the expander could be used for ammonia-water absorption power system with the maximum isentropic efficiency of 61%. They also proposed semi-empirical models to predict the scroll expander performance, and developed equations to calculate the mechanical loss and internal leakage. Iglesias and Favrat [12] developed and validated a theoretical model of an oil-free co-rotating scroll compressor-expander for a small scale compressed air energy storage system, and both the simulated and experimental results suggested the reduction of internal leakage area for performance improvement. Yang et al. [13] used a separate scroll compressor and a scroll expander to build a micro-compressed air energy storage system, as the simulation and the test results showed that the energy conversion efficiency of the expander was about 23–36% when the air supply pressure was at 3.5–6.5 bar. Gao et al. [14] applied the scroll expander to a fuel cell work recovery system, and the test results showed the considerable influence of scroll internal leakage on the recovery efficiency. Moreover, Bao et al. [15] and Jiang et al. [16] applied scroll expander to chemisorption refrigeration and power cogeneration systems. They have successfully demonstrated this novel combination and obtained a few hundred Watt electricity output together with about 3.0 kW refrigeration output.

The modelling and simulation of scroll expander was considered as sophisticated due to the complicated scroll geometry. The majority of numerical investigation on scroll expander (or compressor) was based on thermodynamic methodology, which solves thermodynamic states of the working fluid at each point of the scroll rotation. Wang et al. [17–19] published a series of numerical simulation and experimental studies on a scroll air motor, including geometry description and torque analysis [17], development of mass and energy balance equations and experimental test results [18,19]. Their scroll expander model was coupled with the model of a direct current (DC) or an alternating current (AC) generator, and the simulation results showed good agreement with the experimental data as the overall thermal efficiency was 35–55% depending on the inlet air pressure and electric load resistance. Liu et al. [20,21] verified their scroll expander model by testing with compressed air and R123 as working fluid. To supplement the model, the authors pre-tested the used generator to develop empirical correlation between mechanical friction torque and rotational speed. The volume efficiency of the scroll expander was found 0.38–0.68 with a rotational speed range of 1200–2800 rev min^{-1}. Kim et al. [22] modelled a scroll expander and obtained its adiabatic and mechanical efficiencies through the gas force analysis and the establishment of the force and momentum balance equations for each moving part of the scroll expander. The simulation results indicated an improvement of the total expander efficiency by 65% via reducing the scroll internal leakage clearance by half.

Apart from the thermodynamic methodology, lumped method and CFD (Computational Fluid Dynamic) approach have also been adopted to develop numerical model of scroll expander. The lumped method neglects the state changes of the working fluid inside the expander but treats the expander as a lump unit, while the essential parameters can be determined through experimental tests. The model reported by Lemort et al. [4,6] and Quoilin et al. [7] are based on this lumped method, and the evolution of the working fluid was decomposed to several steps, including adiabatic supply pressure drop, isobaric supply cooling down, adiabatic and reversible expansion with the build-in volume ratio, adiabatic expansion in constant volume, adiabatic mixing between main working fluid and leakage flow, and isobaric exhaust cooling down. The authors experimentally validated their model, and the maximum deviation between the simulated and experimental results was 2% on mass flow rate while it was 6% on shaft power. Giuffrida [23] adopted Lemort et al. [6]'s models to evaluate a micro ORC system using several working fluids, and the results suggested R141b as a better alternative working fluid for R123. Chang et al. [24] simulated scroll expander using CFD method as the scroll geometric model was built and meshed in the two-dimensional planar while the mass, momentum and energy equations were solved by k-ε method. Two types of scroll expanders have been experimentally tested to validate the CFD-based simulation, and the results showed that the CFD method overestimated the scroll expander performance because the scroll wrap was idealised somehow in the modelling. Song et al. [25] conducted three-dimension CFD simulation to study the impact of suction port configuration and location on the dynamic performance of a scroll expander, where R123 was used as the working fluid in a small scale ORC system.

So far the modelling method of scroll expander – generator system has broad diversity due to different scroll structures, different generator types, different specific focus and different definitions of the system configurations and working processes. In this paper, a detailed and generic dynamic modelling and simulation method of scroll expander is presented step by step. Scroll geometry models, valve model, internal leakage model, motion equation, heat transfer equation and energy balance equation are combined to complete a scroll expander model. The generality of the present model is embodied in a unique approach to acquire the mechanical friction loss in the expander – generator system, which is one of significantly influential factors to the expander performance but difficult to estimate. Some of the aforementioned studies treated it as a constant value but in fact it is a varying parameter dependent on operational conditions; some used elaborated equations to calculate the friction coefficient of each moving part, which would further require more mechanism information and detailed mathematic description of scroll components, and it is very likely to become cumbersome to manipulate. The present work proposes to use an overall dynamic friction coefficient of scroll expander and generator to simplify the parametric system with more realistic friction data, which can be determined by the experimental results and then be used to simulate system performance over a wider range of operational conditions. The present model and simulation method have been validated by present experiments and two other sets of experimental works based on different scroll expanders reported by other researchers [18,20], which verified its broad adaptability for different expander – generator systems.

2. Geometry description of scroll expander

2.1. Involute of circle

Spiral is the fundamental geometry of the scroll. Shown in Fig. 1 is the involute of a circle, which is the most commonly used scroll

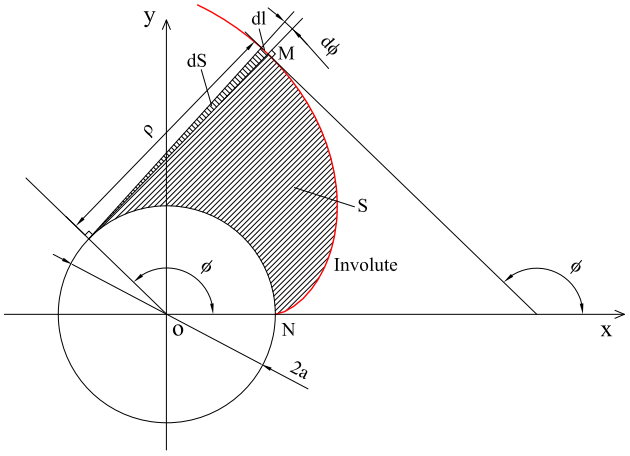

Fig. 1. Involute of a circle.

spiral. The coordinates of this involute are dominated by the equations as Eqs. (1) and (2).

$$x = a(\cos\phi + \phi\sin\phi) \tag{1}$$

$$y = a(\sin\phi - \phi\cos\phi) \tag{2}$$

where a is the basic circle radius, ϕ is the involute angle (corresponding to a point M in the figure). The radius of the involute, ρ, at point M is then calculated by Eq. (3).

$$\rho = \sqrt{x^2 + y^2 - a^2} = \sqrt{a^2(1+\phi^2) - a^2} = a\phi \tag{3}$$

The differential length of the involute, dl, and the differential area, dS can be calculated by the following Eqs. (4) and (5) respectively.

$$\mathrm{d}l = \rho\mathrm{d}\phi = a\phi\mathrm{d}\phi \tag{4}$$

$$\mathrm{d}S = \frac{1}{2}(a\phi)^2\mathrm{d}\phi \tag{5}$$

By integrating dl and dS from 0 to ϕ, the involute length, l, from the start point N to point M and the area between involute and basic circle, S, can be calculated using Eqs. (6) and (7) respectively.

$$l = f_l(\phi) = \int_0^{\phi} a\phi\,\mathrm{d}\phi = \frac{1}{2}a\phi^2 \tag{6}$$

$$S = f_S(\phi) = \int_0^{\phi} \frac{1}{2}(a\phi)^2\mathrm{d}\phi = \frac{1}{6}a^2\phi^3 \tag{7}$$

2.2. Scroll geometry

Two identical scroll wraps are used to form the scroll expander, as shown in Fig. 2. One of the scroll wraps is stationary and is called fixed scroll; while the other one is placed by rotating the fixed scroll by 180°, and is named as orbiting scroll since it is the only one rotates. The inner and outer scroll edges are the involutes of the basic circle with involute angles of α and $-\alpha$, respectively. The coordinates of these two involutes (x_i, y_i) and (x_o, y_o) are given by Eqs. (8)–(11).

$$x_i = a(\cos\phi_i + (\phi_i - \alpha)\sin\phi_i) \tag{8}$$

$$y_i = a(\sin\phi_i - (\phi_i - \alpha)\cos\phi_i) \tag{9}$$

$$x_o = a(\cos\phi_o + (\phi_o + \alpha)\sin\phi_o) \tag{10}$$

$$y_o = a(\sin\phi_o - (\phi_o + \alpha)\cos\phi_o) \tag{11}$$

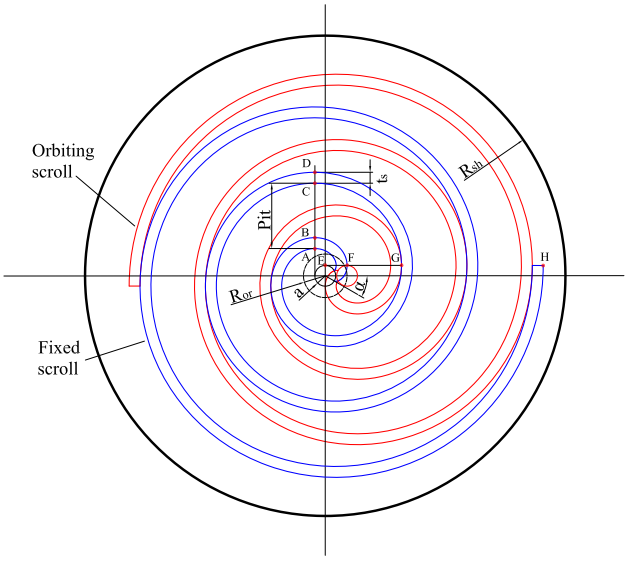

Fig. 2. Scroll geometric parameters.

Points A to H in Fig. 2 are illustrated to help calculate scroll geometric parameters. Points A and B have an involute angle of π while points C and D are at 3π. According to Eqs. (8)–(11), the coordinates of points A to D are

$$\mathrm{A}(-a, a(\pi-\alpha)),\ \mathrm{B}(-a, a(\pi+\alpha)),\ \mathrm{C}(-a, a(3\pi-\alpha)),\ \mathrm{D}(-a, a(3\pi+\alpha))$$

Therefore the scroll thickness, t_s, and the pitch, *Pit*, shown in the figure can be determined by the length of line segments AB (or CD) and AC (or BD), respectively as the following equations.

$$t_s = 2a\alpha \tag{12}$$

$$Pit = 2\pi a \tag{13}$$

Point G is one of the mesh points of the orbiting scroll and the fixed scroll, which has an involute angle of 3π/2 for orbiting scroll (outer involute) and 5π/2 for fixed scroll (inner involute). To achieve perfect meshing, the orbiting radius, R_{or}, which has the equal value of the length of line segment EF, must satisfy the following equation.

$$R_{or} = l_{GE} - l_{GF} = a\left(\frac{5}{2}\pi - \alpha\right) - a\left(\frac{3}{2}\pi + \alpha\right) = \pi a - 2a\alpha \tag{14}$$

As seen from the figure, the end involute angle is $\phi_e = (2N_C + 1/2)\pi$, where N_C is the number of expansion chamber pairs. Hence the point H, which is the end point of outer involute of the fixed scroll, has the coordinate of $((\phi_e + \alpha)a, a)$. Involving the orbiting radius R_{or}, the radius of the shell shown in the figure is calculated by Eq. (15).

$$R_{sh} = \sqrt{(a(\phi_e + \alpha) + R_{or})^2 + a^2} \tag{15}$$

2.3. Rotation of the scroll

During the scroll expander operation, the orbiting scroll rotates anticlockwise along a circular orbit with a radius of R_{or} without rotating around its own axis. Fig. 3 exemplifies an operational cycle of a scroll expander with 3 pairs of expansion chambers (① to ③ as shown in the figure) and one discharge chamber. The orbiting angle, θ, is defined as the angle between the horizontal axis and the connection line from the basic circle centre of the fixed scroll to the basic circle centre of the orbiting scroll. At the very begin-

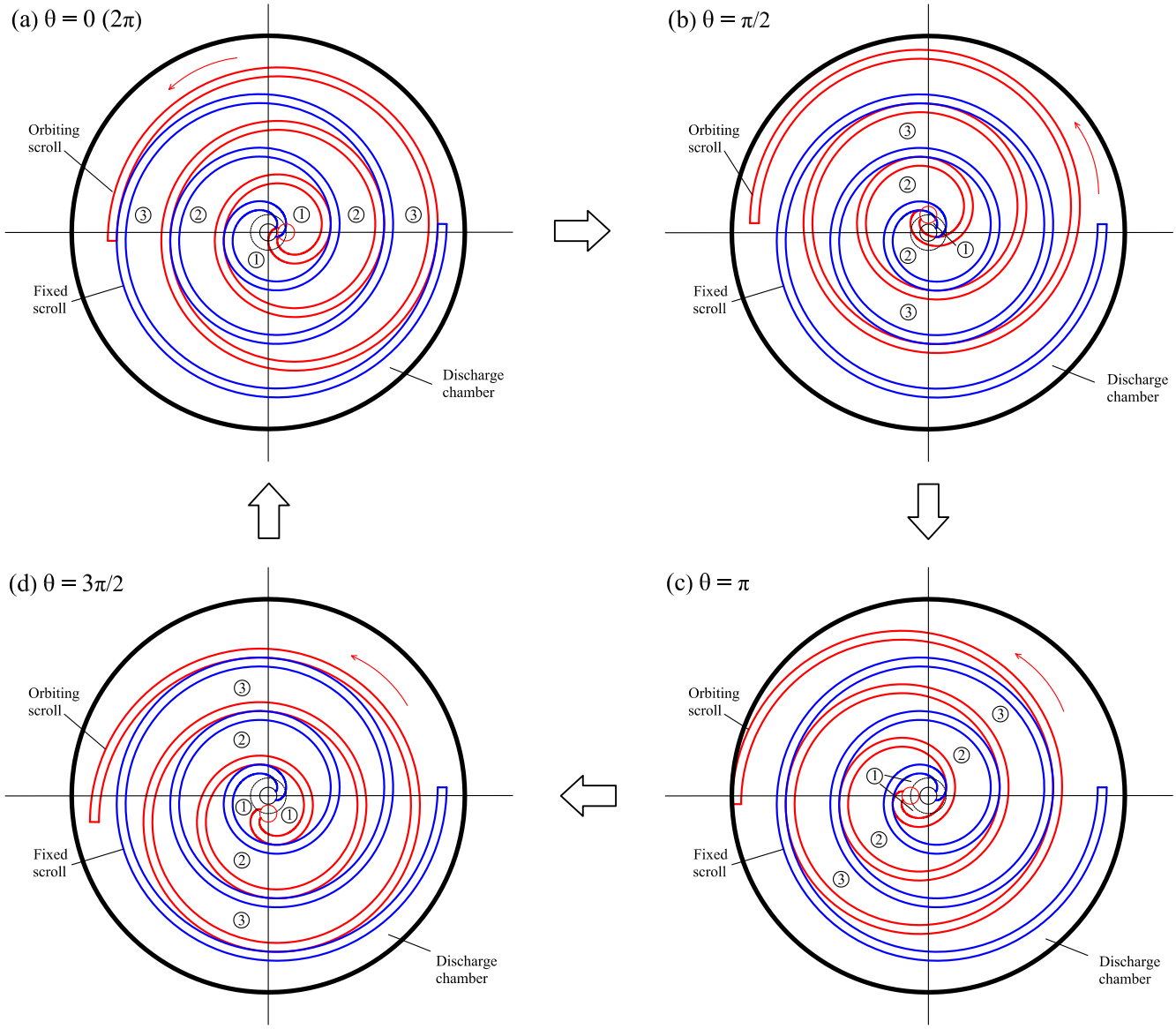

Fig. 3. Operational cycle of a scroll expander with three pairs of expansion chambers.

ning, $\theta = 0$ (or $\theta = 2\pi$), all the expansion chambers reach their maximum volume after previous rotation, while the discharge chamber has its minimum volume, as illustrated in Fig. 3(a). When the orbiting scroll rotates, new chamber 1 is formed, the volume of which starts from 0; the previous chamber 1 becomes new chamber 2; the previous chamber 2 becomes new chamber 3; and the previous chamber 3 merges with the previous discharge chamber. As the orbiting scroll keeps rotating, the expansion chambers 1–3 expand while the discharge chamber is compressed due to the constant total volume inside the expander shell, as shown in Fig. 3(b)–(d). When a rotation circle is finished, all the chambers reach their initial states as $\theta = 2\pi$ (or $\theta = 0$).

Fig. 4 is shown to assist in understanding the position of each mesh point between fixed and orbiting scrolls. At an orbiting angle θ, points K and L are the mesh points between chamber 1 and chamber 2, M and N are the mesh points between chamber 2 and 3 while points O and P separate chamber 3 and the discharge chamber. The involute angle of point K at the fixed scroll, ϕ_K, equals to $\theta - \pi/2$ as considering the perpendicular relationship between the tangent line of scroll involute at the mesh point and the connection line of O_1O_2. Thereafter more mesh points at the fixed scroll can be consecutively added in the increment of π. Meanwhile, the involute angles of these mesh points at orbiting scroll are mirrored against those at fixed scroll, as summarized in Table 1, where F and F′ are the points on the inner and outer involutes of the fixed scroll respectively, and O and O′ are the points on the inner and outer involutes of the orbiting scroll respectively. More generally, the involute angles of mesh points can be determined by the following method, where i is the chamber number.

Fixed scroll: F′ $(-\pi/2 + \theta + 2(i-1)\pi)$ F $(\pi/2 + \theta + 2(i-1)\pi)$
Orbiting scroll: O $(\pi/2 + \theta + 2(i-1)\pi)$ O′ $(-\pi/2 + \theta + 2(i-1)\pi)$.

2.4. Modification of the scroll profile

The geometry of the scroll needs to be modified to achieve high efficiency, light weight and easy manufacture. Fig. 5 shows two typical modification methods. Fig. 5(a) shows the scroll profile modified by a circular cutter, the intersect area between the cutter and the scroll is removed. The cutter circle centre is the cross point of the basic circle and the left side of x coordinate, hence the

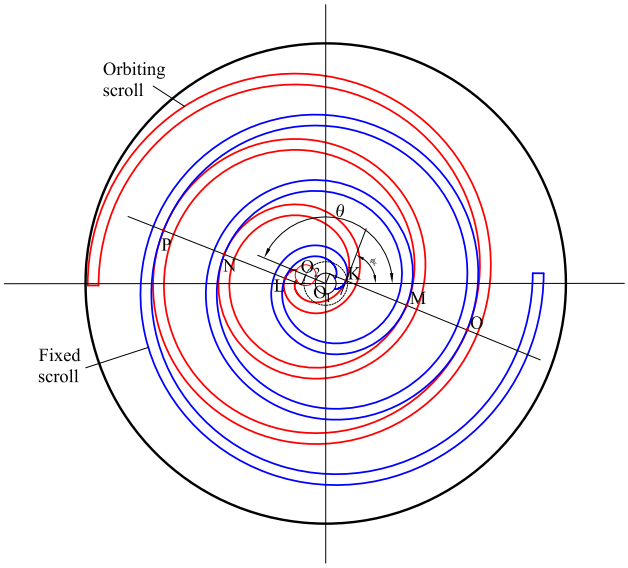

Fig. 4. Mesh points of fixed and orbiting scroll wraps.

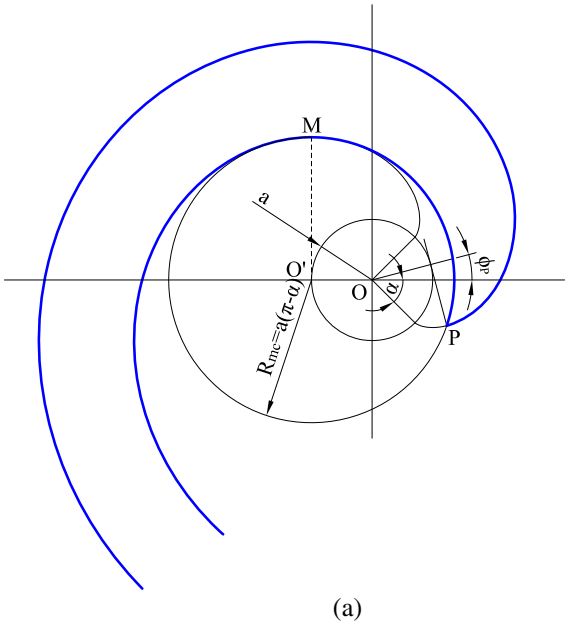

maximum radius of the cutter is $R_{mc} = a(\pi - \alpha)$ as shown in the figure. Eq. (16) governs the cutter circle.

$$(x + a)^2 + y^2 = a^2(\pi - \alpha)^2 \tag{16}$$

The new-formed scroll wrap has a sharp corner, as shown by point P in the figure, the involute angle of which can be calculated by substituting Eqs. (10) and (11) for x and y respectively in Eq. (16), therefore it evolves to Eq. (17) and further to Eq. (18) after simplification.

$$(a(\cos\phi_P + (\phi_P + \alpha)\sin\phi_P) + a)^2 + (a(sin\phi_P - (\phi_P + \alpha)\cos\phi_P))^2 = a^2(\pi - \alpha)^2 \tag{17}$$

$$(\phi_P + \alpha)^2 + 2\cos\phi_P + 2(\phi_P + \alpha)\sin\phi_P = (\pi - \alpha)^2 - 2 \tag{18}$$

Due to this modification, the volume of chamber 1 is not zero at $\theta = 0$ since it is connected to chamber 2 through the emerged clearance caused by the missing of mesh points between these two chambers. These two chambers will be disconnected when point P becomes the mesh point. Thus, the disconnecting orbiting angle, θ_{disc}, can be determined by considering point P to be the mesh point F′ $(-\pi/2 + \theta + 2(i-1)\pi)$ with $i = 1$. The following expression is then given to calculate the disconnection rotational angle, θ_{disc}

$$\theta_{disc} = \phi_P + \frac{\pi}{2} \tag{19}$$

From a mechanical point of view, the sharp corner of the scroll is unfavourable due to the high stress concentration at this corner. Fig. 5(b) shows another modification method by the so-called perfect mesh profile (PMP) [26,27], as the modifying curve consists of two circular arcs, which are all tangential with the involutes at contact points, leading to smooth and continuous profile. To ensure the perfect mesh of two scrolls, the two arcs must have the same unfold angle, λ, as shown in Fig. 5(b). Point A with an involute angle

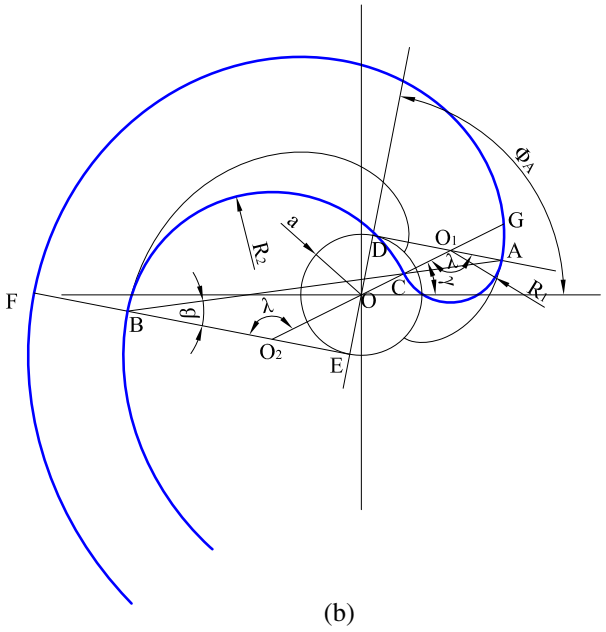

Fig. 5. Scroll modification methods, (a) modification by a cutter; (b) modification by PMP.

ϕ_A at the outer involute of the scroll should be pre-selected as the start position of the modification; while the end position of the modification is point B at inner involute with an involute angle of $(\pi + \phi_A)$. These two arcs have the diameters of R_1 and R_2 respectively, and the circle centre connection line O_1O_2 must cross the basic circle centre point O. Because of the congruence of triangles ΔODO_1 and ΔOEO_2, $l_{OO_1} = l_{OO_2}$ and $l_{O_1D} = l_{O_2}E$, the following expressions of R_1 and R_2 can be obtained.

Table 1
Mesh points at inner and outer involutes of fixed and orbiting scroll wraps.

	Point K	Point L	Point M	Point N	Point O	Point P
Fixed scroll	F′ $(-\pi/2 + \theta)$	F $(\pi/2 + \theta)$	F′ $(3\pi/2 + \theta)$	F $(5\pi/2 + \theta)$	F′ $(7\pi/2 + \theta)$	F $(9\pi/2 + \theta)$
Orbiting scroll	O $(\pi/2 + \theta)$	O′ $(-\pi/2 + \theta)$	O′ $(5\pi/2 + \theta)$	O′ $(3\pi/2 + \theta)$	O $(9\pi/2 + \theta)$	O′ $(7\pi/2 + \theta)$

$$R_2 - R_1 = R_2 - R_1 + l_{O_2E} - l_{O_1D} = l_{BE} - l_{AD} = \rho(B) - \rho(A) = R_{or} \tag{20}$$

$$l_{OC} = l_{OO_1} - R_1 = R_2 - l_{OO_2} = \frac{R_2 - R_1}{2} = \frac{R_{or}}{2} \tag{21}$$

$$R_1 = l_{OO_1} - l_{OC} = \frac{a}{\sin(\pi - \lambda)} - \frac{R_{or}}{2} = a\left(\frac{1}{\sin\lambda} + \alpha - \frac{\pi}{2}\right) \tag{22}$$

$$R_2 = R_1 + R_{or} = a\left(\frac{1}{\sin\lambda} - \alpha + \frac{\pi}{2}\right) \tag{23}$$

The angles including λ, β and γ in Fig. 5(b) must be calculated to complete the modification, which can be derived by the following steps.

$$l_{O_1D} = \rho(A) - R_1 = a(\phi_A + \alpha) - a\left(\frac{1}{\sin\lambda} + \alpha - \frac{\pi}{2}\right) = a\left(\phi_A - \frac{1}{\sin\lambda} + \frac{\pi}{2}\right) \tag{24}$$

$$l_{O_1D} = a\cot(2\beta) \tag{25}$$

$$\cot(2\beta) = \phi_A - \frac{1}{\sin\lambda} + \frac{\pi}{2} = \phi_A - \frac{1}{\sin(\pi - 2\beta)} + \frac{\pi}{2} \tag{26}$$

$$\cot\beta = \phi_A + \frac{\pi}{2} \tag{27}$$

$$\lambda = \pi - 2\beta \tag{28}$$

$$\gamma = \phi_A - \left(\frac{\pi}{2} - (\pi - \lambda)\right) = \phi_A + \frac{\pi}{2} - \lambda \tag{29}$$

Similar to the modification by circular cutter, PMP modification results in the connection of the chamber 1 and 2 at the very beginning of the scroll rotation. The disconnection orbiting angle for such modification profile is equal to γ as both the fixed scroll and orbiting scroll are meshed at the same point C.

2.5. Volume of scroll chamber

Except chamber 1, each expansion chamber is enclosed by the inner involute of one scroll and outer involute of the other scroll between two mesh points. Taking the left side part of chamber 2 in Fig. 4 as an example, the chamber is enclosed by the outer involute of fixed scroll and inner involute of orbiting scroll from mesh point K to M. Based on area calculation, Eq. (7), the enclosed area of this part of chamber 2 can be calculated by the following equation

$$\begin{aligned} S_{C2-left} &= f_S(O(M)) - f_S(O(K)) - [f_S(F'(M)) - f_S(F'(K))] \\ &= \frac{1}{6}a^2\left[(\phi_{M\text{-}o} - \alpha)^3 - (\phi_{K\text{-}o} - \alpha)^3\right] - \frac{1}{6}a^2\left[(\phi_{M\text{-}f} + \alpha)^3 - (\phi_{K\text{-}f} + \alpha)^3\right] \end{aligned} \tag{30}$$

where the subscripts M-o, K-o, M-f, K-f indicate the point M and K at orbiting scroll and fixed scroll respectively. Using the involute angle given in Table 1, Eq. (30) becomes

$$\begin{aligned} S_{C2-left} &= \frac{1}{6}a^2\left[\left(\frac{5\pi}{2} + \theta - \alpha\right)^3 - \left(\frac{\pi}{2} + \theta - \alpha\right)^3\right] \\ &\quad - \frac{1}{6}a^2\left[\left(\frac{3\pi}{2} + \theta + \alpha\right)^3 - \left(-\frac{\pi}{2} + \theta + \alpha\right)^3\right] \end{aligned} \tag{31}$$

$$S_{C2-left} = 2\pi a^2(\pi + \theta)(\pi - 2\alpha) \tag{32}$$

Hence, the volume of the total chamber 2 is calculated by

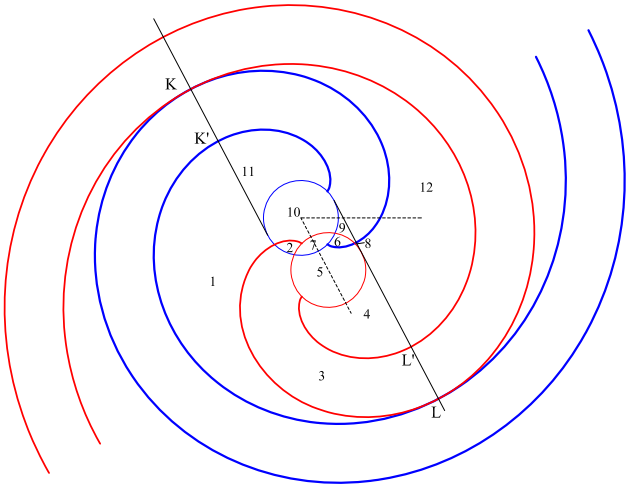

Fig. 6. Area of chamber 1.

$$V_{C2} = 2h_sS_{C2-left} = 4\pi a^2h_s(\pi + \theta)(\pi - 2\alpha) \tag{33}$$

where h_s is the scroll height. More general calculation in area and volume ($2 \leqslant i \leqslant N_C$) can be derived as

$$\begin{aligned} S_{Ci} &= 2\left[f_S\left(\frac{\pi}{2} + \theta - \alpha + 2(i-1)\pi\right) - f_S\left(\frac{\pi}{2} + \theta - \alpha + 2(i-2)\pi\right)\right. \\ &\quad \left. - f_S\left(-\frac{\pi}{2} + \theta + \alpha + 2(i-1)\pi\right) + f_S\left(-\frac{\pi}{2} + \theta + \alpha + 2(i-2)\pi\right)\right] \\ &= \frac{a^2}{3}\left[\left(\frac{\pi}{2} + \theta - \alpha + 2(i-1)\pi\right)^3 - \left(\frac{\pi}{2} + \theta - \alpha + 2(i-2)\pi\right)^3\right] \\ &\quad - \frac{a^2}{3}\left[\left(-\frac{\pi}{2} + \theta + \alpha + 2(i-1)\pi\right)^3 - \left(-\frac{\pi}{2} + \theta + \alpha + 2(i-2)\pi\right)^3\right] \\ &= 4\pi a^2(\pi - 2\alpha)(\theta - 3\pi + 2i\pi) \end{aligned} \tag{34}$$

$$V_{Ci} = h_sS_{Ci} = 4\pi a^2h_s(\pi - 2\alpha)(\theta - 3\pi + 2i\pi) \tag{35}$$

The area and volume of chamber 1 can be determined by the geometric method with the aid of Figs. 6 and 7. As shown in Fig. 6, the area of chamber 1 and parts of scroll wrap at an arbitrary orbiting angle are divided into 12 individual small pieces, then the total area of chamber 1 can be expressed as

$$S_{C1} = A_1 + A_4 + A_5 + A_7 + A_8 + A_{10} + A_{11} + A_{12} \tag{36}$$

Eq. (36) can be simplified to Eq. (37) as some elements are in symmetry, $A_1 = A_{12} + A_8$, $A_{11} = A_4$, $A_2 = A_6$, $A_5 = A_{10}$.

$$S_{C1} = 2(A_1 + A_4 + A_5) + A_7 \tag{37}$$

The area S_{11} in Fig. 7(a), enclosed by basic circle and inner involute of fixed scroll between two mesh points L and K, can be calculated by Eq. (38). The calculation of area S_{12} in Fig. 7(b) is given as Eq. (39). The area S_{13} representing the difference area value between the shadow area and the yellow[1] area shown in Fig. 7(c) can be obtained using Eq. (40).

$$\begin{aligned} S_{11} &= A_1 + A_3 + A_4 + A_5 + A_6 + A_8 + A_9 = f_s(F(L)) - f_s(F(K')) \\ &= \frac{a^2\left(\left(\frac{\pi}{2} + \theta - \alpha\right)^3 - \left(-\frac{\pi}{2} + \theta - \alpha\right)^3\right)}{6} \end{aligned} \tag{38}$$

[1] For interpretation of color in Fig. 7, the reader is referred to the web version of this article.

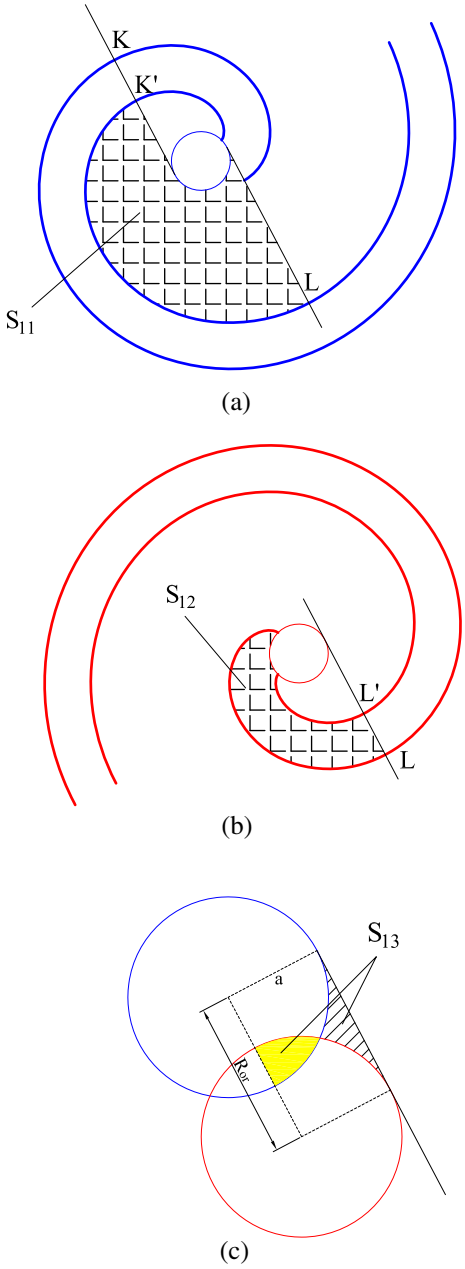

Fig. 7. Divided area of chamber 1, (a) S_{11}; (b) S_{12}; (c) S_{13}.

$$S_{12} = A_3 + A_2 = A_3 + A_6 = f_s(O'(L)) - f_s(O(L')) = \frac{a^2\left(\left(-\frac{\pi}{2}+\theta+\alpha\right)^3 - \left(-\frac{\pi}{2}+\theta-\alpha\right)^3\right)}{6} \tag{39}$$

$$S_{13} = A_8 + A_9 - \frac{A_7}{2} = R_{or}a - \frac{\pi a^2}{2} = \frac{a^2}{2}(\pi - 4\alpha) \tag{40}$$

Therefore the area S_{C1} and volume V_{C1} can be derived as Eqs. (41) and (42).

$$S_{C1} = 2(S_{11} - S_{12} - S_{13}) = \frac{a^2\left[\left(\frac{\pi}{2}+\theta-\alpha\right)^3 - \left(-\frac{\pi}{2}+\theta+\alpha\right)^3\right]}{3} - a^2(\pi - 4\alpha) \tag{41}$$

$$V_{C1} = h_s S_{C1} \tag{42}$$

The volume of the discharge chamber ($i = N_C + 1$) is obtained as

$$V_{dis} = \pi h_s R_{sh}^2 - \sum_{i=1}^{i=N_C} V_{Ci} - 2h_s S_{scroll} \tag{43}$$

where S_{scroll} is the projected area of scroll wrap on the scroll base plate, which can be calculated based on Eq. (7) and therefore has the following expression

$$S_{scroll} = \frac{1}{6}a^2\left[(\phi_e+\alpha)^3 - (\phi_e-\alpha)^3\right] = a^2\alpha\left(\phi_e^2 + \frac{\alpha^2}{3}\right) \tag{44}$$

However, the volume of chamber 1 and chamber 2 need to be re-calculated considering the scroll profile modification. The cut area by the circular cutter and the corresponding increased volume can be calculated by the process given in Appendix A. The volume of chamber 1 and 2 against the orbiting angle are

$$V_{C1\text{-}mc} = V_{C2\text{-}mc} = V_{C1} + V_{C2} + V_{mc} \quad \theta \leqslant \theta_{disc} \tag{45}$$

$$\begin{cases} V_{C1\text{-}mc} = V_{C1} + V_{mc} \\ V_{C2\text{-}mc} = V_{C2} \end{cases} \quad \theta > \theta_{disc} \tag{46}$$

The modification area and volume by using PMP method is given in Appendix B. The volume variations of chamber 1 and chamber 2 are more complex and deduced in detail in Appendix C, the final expressions are presented as follows.

$$V_{C1\text{-}mp} = V_{C2\text{-}mp} = V_{C1} + V_{C2} + V_{mp} \quad \theta \leqslant \gamma \tag{47}$$

$$\begin{cases} V_{C1\text{-}mp} = h_s\left(R_2^2 - R_1^2\right)(\theta - \gamma - \sin(\theta - \gamma)) \\ V_{C2\text{-}mp} = V_{C1} + V_{C2} + V_{mp} - V_{C1\text{-}mp} \end{cases} \quad \gamma < \theta \leqslant \gamma + \lambda \tag{48}$$

$$\begin{cases} V_{C1\text{-}mp} = V_{C1} + V_{mp} \\ V_{C2\text{-}mp} = V_{C2} \end{cases} \theta > \gamma + \lambda \tag{49}$$

3. Mathematic models of scroll expander – generator system

3.1. Valve model

Valves are installed before and after the expander to control the working fluid flow. The standard valve model is recommended by Refs. [28,29] as Eq. (50).

$$\dot{m}_{valve} = N_6 F_P C_v Y \sqrt{x P_u \rho_u} \tag{50}$$

where P_u and ρ_u are the upstream working fluid pressure and density; N_6 is the numerical constant and it is 27.3 when pressure is in the unit of bar and mass flow rate is in the unit of kg h^{-1}; F_P is the piping geometry factor which reflects the pressure loss due to the fittings attached directly to the inlet or outlet of the valve; C_v is the valve capacity coefficient, given by the valve manufacturer; Y is expansion factor accounting for the density change of the compressible fluid, which can be obtained by using Eq. (51).

$$Y = 1 - \frac{x_P}{3F_k x_T} \tag{51}$$

where x_P is the ratio of pressure drop, F_k is the ratio of specific heats factor, x_T is the critical pressure drop ratio factor and should be provided by the valve manufacturer. The following equations are given to calculate x_P and F_k considering the chocked flow

$$x_P = \min\left(\frac{P_u - P_d}{P_u}, F_k x_T\right) \tag{52}$$

$$F_k = \frac{k}{1.4} \tag{53}$$

where k is the isentropic expansion factor (c_p/c_v).

3.2. Internal leakage area and leakage flow

The fixed scroll and orbiting scroll should mesh with each other perfectly during the rotation; however, the internal leakage inside the expander is inevitable in reality. There are mainly two types of leakage between scroll chambers, flank leakage and radial leakage as illustrated in Fig. 8(a) and (b), respectively. The flank leakage goes through the clearance between the side surfaces of two scrolls while the radial leakage goes through the clearance between the tip wall of one scroll and the base plate of the other scroll. The clearance size has been reported by several studies, e.g. Wang et al. [17,18] used constant values for both flank clearance δ_f and radial clearance δ_r at 0.01 mm and 0.015 mm respectively; Liu et al. [20,21] used 0.04 mm as both leakage size; nevertheless, some [30,31] believed the clearances were varying as the changing of pressure difference between chambers.

As the flank leakage on both sides in symmetry, the length of the clearance on each side is the scroll height, thus the total leakage length is

$$L_f = 2h_s \tag{54}$$

For the radial leakage, the clearance is in between two mesh points of the scrolls, hence the length can be calculated based on Eq. (4) and the calculation expression in relation to the chamber number i and orbiting angle θ as given as Eq. (55).

$$L_r = 2\int_{-\frac{\pi}{2}+\theta+2(i-1)\pi}^{\frac{\pi}{2}+\theta+2(i-1)\pi} a\phi\,\mathrm{d}\phi = 2\pi a(2(i-1)\pi+\theta) \tag{55}$$

The mass flow rate of the leakage flow can be referred to the orifice theory since the leakage clearances are quite small compared to the scroll thickness. The following equations are commonly used [14,18,20,21]

$$\dot{m}_r = f_r\delta_r L_r\sqrt{\frac{2k}{k-1}P_i\rho_i\left(\varepsilon^{\frac{2}{k}}-\varepsilon^{\frac{k+1}{k}}\right)} \tag{56}$$

$$\dot{m}_f = f_f\delta_f L_f\sqrt{\frac{2k}{k-1}P_i\rho_i\left(\varepsilon^{\frac{2}{k}}-\varepsilon^{\frac{k+1}{k}}\right)} \tag{57}$$

where f_r and f_f are the flow coefficients of the working fluid, which were recommended by Wang et al. [18] at 0.87–0.95 if the air was the working fluid; i is the chamber number; ε is the expansion ratio which is formulated as Eq. (58) considering the chocked flow.

$$\varepsilon = \max\left(\frac{P_{i+1}}{P_i}, \left(\frac{2}{k+1}\right)^{\frac{k}{k-1}}\right) \tag{58}$$

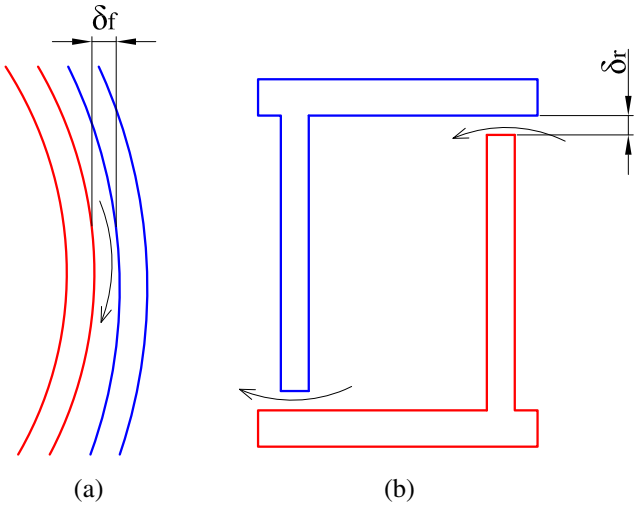

Fig. 8. Internal leakages of scroll expander, (a) flank leakage; (b) radial leakage.

3.3. Motion equation of the orbiting scroll

The pressure difference between two adjacent chambers generates gas forces, including tangent force, radial force and axial force as shown in Fig. 9(a)–(c).

The tangent force is the one that drives the rotation of the orbiting scroll. This force is perpendicular to the connection line O_fO_o and towards the lower pressure chamber, thus the force direction is at an angle of $\theta+\pi/2$. Taking the left side part of chamber 2 in Fig. 9(a) for instance, only part of the orbiting scroll (between mesh points N and M) in this chamber is imposed on the gas force generated by the pressure difference between chamber 2 and 3, while the other part of scroll (between mesh points K and N) does not sustain the gas force since it is facing the right side part of chamber 2. Only the fixed scroll in the right side part of chamber 2 is sub-

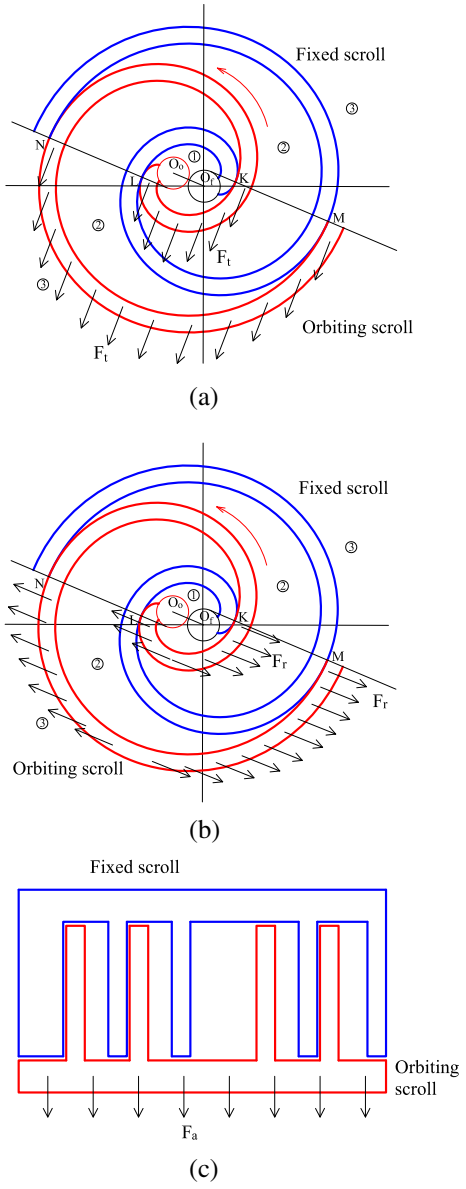

Fig. 9. Forces generated on orbiting scroll, (a) tangent force; (b) radial force; (c) axial force.

jected to the gas force. Ignoring the thickness of the scroll, the tangent force on the orbiting scroll between chambers i and $i+1$ can be calculated by the following equation

$$F_t(i) = (P_i - P_{i+1})h_s[2a(-\pi/2 + \theta + 2(i-1)\pi) + \pi a] = 2h_s a[\theta + 2(i-1)\pi](P_i - P_{i+1}) \quad (59)$$

As shown in Fig. 9(b), the radial force working on the orbiting scroll offsets the majority force by itself, only the part mapping on the basic circle remains. Eq. (60) is used to calculate the radial force related to each chamber.

$$F_r(i) = 2h_s a(P_i - P_{i+1}) \quad (60)$$

The axial force on the orbiting scroll is generated by the pressure difference between two sides of the scroll base plate as shown in Fig. 9(c). The pressure can be calculated by

$$F_a = \sum(P_i S_{Ci}) - P_b S_{orb\text{-}plate} \quad (61)$$

where P_b is the pressure on the other side of orbiting plate.

As aforementioned, the tangent force drives the rotation of orbiting scroll. Every point on the orbiting scroll rotates along a circle at the same diameter R_{or} but with different circular centre, the torque produced by the tangent force on the orbiting scroll can be given as

$$T_t = R_{or}\sum_{i=1}^{N_C} F_t(i) \quad (62)$$

This torque is the driving moment of the rotation, and it conquers the mechanical friction torque T_{fr} to provide the electromechanical torque T_{em} when a generator is connected, therefore the equation describing the expander – generator rotation can be expressed as Eq. (63) [32,33].

$$\left(J_{orb} + J_{sha} + J_{arm} + J_{Old}\sin^2\theta\right)\frac{d\omega}{dt} - J_{Old}\sin\theta\cos\theta\omega^2 = T_t - T_{fr} - T_{em} \quad (63)$$

where J is the inertia moment of the rotating parts, ω is the angular velocity, the subscripts orb, sha, arm and Old indicate the orbiting scroll, the shaft, the generator armature and the Oldham ring (which prevents the self-rotation of the orbiting scroll), respectively. Eq. (64) are given for these inertias.

$$J_{orb} = m_{orb}R_{or}^2,\ J_{sha} = m_{sha}R_{sha}^2/2,\ J_{arm} = m_{arm}(R_{arm\text{-}out}^2 + R_{arm\ \text{-}in}^2)/2,\ J_{Old} = m_{Old}R_{or}^2 \quad (64)$$

Because the Oldham ring performs reciprocating motion along a straight line but not the orbiting circle, its inertia should be modified by involving the rotating inertia along the orbiting circle and the orbiting angle as given in Eq. (63).

The bearings involved in the calculation of mechanical friction torques are illustrated in Fig. 10. Thrust bearings exist on both surfaces of the orbiting scroll base plate. The upper surface receives the thrust load from the cover of the fixed scroll while the lower surface endures the friction with the surface of the supporting frame. The other major friction torques are on the journal bearings which support the crank shaft and the orbiting scroll. Moreover, there is also friction loss between the Oldham ring and its slots. These mechanical friction torques can be calculated by solving force balance equations as reported in [32,34,35], while some experimental tests on friction loss and friction factors have also been reported [36–38]. On the other hand, some studies suggested to use constant mechanical loss [6,39] or linearly varying mechanical loss with rotational speed [4,11]. Mendoza et al. [11] summarized that it was suitable to use a constant mechanical loss to an open-drive expander without generator, whereas the proportional loss should be applied if an electric generator was connected to the

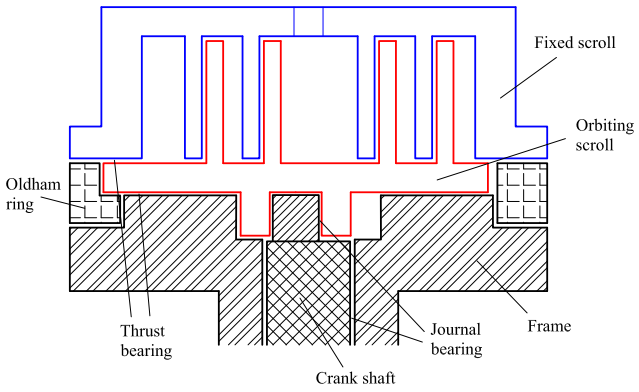

Fig. 10. Schematic of mechanical frictions of the orbiting scroll.

expander since the loss in generator was proportional to the generated power. The authors also reported a nearly linear increase of torque loss between 0.1 N m to 0.6 N m as the rotational speed increasing from 1536 rev min^{-1} to 3018 rev min^{-1}.

3.4. Motion equation of the generator

For a DC (direct current) motor, the electromechanical torque T_{em} is generated when the conductors are placed in a magnetic field and the current flows through these conductors. T_{em} can be calculated by the following equation [40]

$$T_{em} = K_t I_a \quad (65)$$

where K_t is the torque constant, I_a is the charged current from the motor terminal. Eq. (65) can also be applied to a generator. On the other side, the generated current and the angular speed is correlated by Eq. (66) [40].

$$E_a = K_e\omega = (R_{arm} + R_{load})I_a + L_a\frac{dI_a}{dt} \quad (66)$$

where E_a is the back electromotive force (EMF), K_e is the constant of back EMF, L_a is the armature inductance, R_a and R_{load} are the resistances of the armature and electric load respectively. K_e and K_t have the same value if the SI unit is used [40]. The literature [19] can be referred to for an AC (alternative current) generator as the modelling of electromechanical torque is more sophisticated.

Eq. (67) suggested by [40,41] as the motion equation of a DC motor can be used to describe the rotation of a DC generator.

$$T_{Drive} = (J_{arm} + J_{sha})\frac{d\omega}{dt} + B\omega + T_{em} \quad (67)$$

where T_{Drive} is the torque transmitted from the shaft, B is the viscous friction coefficient. The element representing the mechanical friction loss in Eq. (67) is expressed as the multiplication product of a friction coefficient and the rotational speed. Likewise, in the same principle, the present model uses Eq. (68) to describe the sum of friction torque in both scroll and generator to represent T_{fr} in Eq. (63).

$$T_{fr} = f_{SG}\omega \quad (68)$$

where f_{SG} is the proposed overall dynamic friction coefficient of the scroll – generator system, in unit of N m s. Up to the authors' best knowledge, the value of this parameter has not been ever reported. f_{SG} must be pre-determined, and its accurate value was acquired by fitting the experimental data in this work.

3.5. Energy equation of the working fluid

The energy equation of the working fluid in the expansion chambers and discharge chamber is built according to the first law of thermodynamics

$$\frac{\mathrm{d}(mu)}{\mathrm{d}t} = \dot{Q} - \dot{W} + \dot{m}_{\text{C-in}} h_{\text{C-in}} - \dot{m}_{\text{C-out}} h_{\text{C-out}} \tag{69}$$

where m is the working fluid mass in the chamber, u is the specific internal energy, $\dot{Q}$ is the heat transfer rate to the chamber, $\dot{W}$ is the work output rate from the expansion; $\dot{m}_{\text{C-in}}$ and $\dot{m}_{\text{C-out}}$ are the inlet and outlet mass flow rates of working fluid, and $h_{\text{C-in}}$ and $h_{\text{C-out}}$ are the corresponding specific enthalpies. Considering the work output equals to $P\mathrm{d}V/\mathrm{d}t$, the enthalpy $h = u + pV/m$, while the outlet enthalpy of the working fluid $h_{\text{C-out}}$ equals to the chamber enthalpy h_{C}, the above equation can be re-written as

$$\frac{\mathrm{d}(mh_{\text{C}})}{\mathrm{d}t} = \dot{Q} + V\frac{\mathrm{d}P}{\mathrm{d}t} + \dot{m}_{\text{C-in}} h_{\text{C-in}} - \dot{m}_{\text{C-out}} h_{\text{C}} \tag{70}$$

During the expander rotation, the working fluid in each chamber exchange heat with the scrolls and base plates. In order to calculate the heat transfer rate, the heat transfer coefficient of the working fluid is necessary. Jang and Jeong [42] experimentally analogized the heat transfer associating with the scroll rotation to the heat transfer in a rectangular duct with a fixed heating wall and an oscillating wall. The corresponding empirical heat transfer correlation was then given as

$$Nu = \left(1 + 3.5\frac{D_{\text{h}}}{D_{\text{c}}}\right)\left(1 + 8.8\left(1 - e^{-5.35St}\right)\right)Nu_{\text{DB}} \tag{71}$$

The term inside the first bracket on the right side of the correlation is the factor concerning the curved duct, D_{h} is the hydraulic diameter of the flow duct and D_{c} is the mean diameter of the scroll curvature, which can be calculated by Eq. (72) for each chamber i at an orbiting angle θ.

$$\begin{aligned} D_{\text{c}} &= a[(\pi/2 + \theta + 2(i-1)\pi) + (-\pi/2 + \theta + 2(i-1)\pi)] \\ &= 2a(\theta + 2(i-1)\pi) \end{aligned} \tag{72}$$

The term in the second bracket on the right side of Eq. (71) is the correct factor for the oscillating movement, where St is the Strouhal number, a non-dimensional frequency factor as given in Eq. (73).

$$St = \frac{f_{\text{o}} A_{\max}}{\overline{U}} \tag{73}$$

where f_{o} is the oscillating frequency, $A_{\max}$ is the oscillating amplitude, $\overline{U}$ is the mean flow velocity of the working fluid. For a scroll expander, these two factors can be given as

$$f_{\text{o}} = \frac{\omega}{2\pi} \tag{74}$$

$$A_{\max} = R_{\text{or}} \tag{75}$$

Here, $A_{\max}$ is set at R_{or} since $2R_{\text{or}}$ is the maximum flow duct width in the scroll expander. Thus the flow duct in the scroll chamber is analogized to a rectangular duct with varying width from 0 to $2R_{\text{or}}$ and scroll height h_{s}. Therefore, the mean hydraulic diameter and mean flow velocity can be calculated by

$$D_{\text{h}} = \frac{2R_{\text{or}} h_{\text{s}}}{R_{\text{or}} + h_{\text{s}}} \tag{76}$$

$$\overline{U} = \frac{\dot{m}_{\text{total}}}{R_{\text{or}} h_{\text{s}} \rho} \tag{77}$$

Nu_{DB} in Eq. (71) is the Dittus-Boelter heat convection correlation as expressed in Eq. (78).

$$Nu_{\text{DB}} = 0.023 Re^{0.8} Pr^{1/3} \tag{78}$$

By neglecting heat capacity of the scroll wraps and base plates, the heat transfer rate into the working fluid in chamber i is

$$\begin{aligned} \frac{\mathrm{d}Q_i}{\mathrm{d}t} = &\frac{T_{\text{Ci+1}} - T_{\text{Ci}}}{\frac{t_{\text{s}}}{\lambda_{\text{scroll}}} + \frac{D_{\text{h}}}{Nu_{\text{Ci+1}}\lambda_{\text{WF}}} + \frac{D_{\text{h}}}{Nu_{\text{Ci}}\lambda_{\text{WF}}}} A_i + \frac{T_{\text{Ci-1}} - T_{\text{Ci}}}{\frac{t_{\text{s}}}{\lambda_{\text{scroll}}} + \frac{D_{\text{h}}}{Nu_{\text{Ci-1}}\lambda_{\text{WF}}} + \frac{D_{\text{h}}}{Nu_{\text{Ci}}\lambda_{\text{WF}}}} A_{i-1} \\ &+ \frac{T_{\text{amb}} - T_{\text{Ci}}}{\frac{t_{\text{Plate}}}{\lambda_{\text{Plate}}} + \frac{1}{\alpha_{\text{amb}}} + \frac{D_{\text{h}}}{Nu_{\text{Ci}}\lambda_{\text{WF}}}} A_{\text{pi}} \end{aligned} \tag{79}$$

where λ_{scroll} and λ_{WF} are the thermal conductivities of the scroll material and working fluid respectively, λ_{Plate} is the thermal conductivity of the base plate material; t_{s} and t_{Plate} are the thicknesses of the scroll and scroll base plate respectively; α_{amb} is the ambient natural convection heat transfer coefficient. For chamber 1, the second term on the right hand side of Eq. (79) disappears; for the discharge chamber, the downstream temperature $T_{\text{Ci+1}}$ is the ambient temperature T_{amb}, while the heat transfer coefficient term

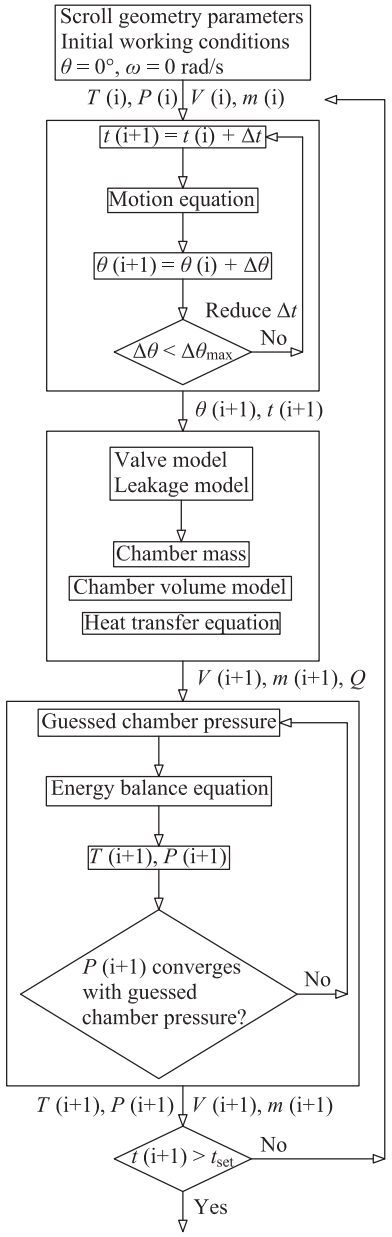

Fig. 11. Flow chart of the simulation process.

Table 2
Parameters used in scroll expander simulation example.

Scroll parameters	
a	3 mm
α	38.2°
t_s	4 mm
Pit	18.8 mm
h_s	30 mm
R_{or}	5.4 mm
N_C	2
J_{orb}	5.85×10^{-6} kg m^2
J_{Old}	9.0×10^{-7} kg m^2
δ_r, δ_f	0.01 mm
f_r, f_f	0.9
Generator parameters (DC generator)	
$J_{sha} + J_{arm}$	2.0×10^{-4} kg m^2
R_a	0.5 Ω
R_{load}	10 Ω, 15 Ω, 20 Ω
K_e, K_t	0.12 N m A^{-1}
L_a	0.0006 H
f_{SG}	0.003 N m s
Valve parameters	
C_v	36[a]
x_T	0.86[a]
Working conditions	
Working fluid	Air
P_{in}	2.5–3.5 bar
T_{in}	80 °C
P_b	1.013 bar
T_b	20 °C

[a] These values are for 1 in. ball valve, 90° open [29].

$D_h/(Nu_{Ci+1}\lambda_{WF})$ in the denominator changes to $1/\alpha_{amb}$. The heat transfer area between chambers is

$$\begin{cases} A_i = L_r h = 2\pi a h_s (2(i-1)\pi + \theta) & i \leqslant N_C \\ A_i = 2\pi R_{sh} h_s & i = N_C + 1 \end{cases} \quad (80)$$

The heat transfer area between chamber and scroll base plate is

$$A_{Pi} = \frac{2V_{Ci}}{h_s} \quad (81)$$

3.6. Power output and efficiencies of scroll expander

Based on the thermodynamics, the total input energy of the working fluid can be calculated by

$$P_{WF} = \dot{m}_{in} h_{in} - \dot{m}_{out} h_{out} \quad (82)$$

where $\dot{m}_{in}$ and $\dot{m}_{out}$ are the inlet and outlet mass flow rates, h_{in} and h_{out} are the corresponding specific enthalpies. The shaft power, P_{sha}, which stands for the power output from the crank shaft to drive the generator is calculated by

$$P_{sha} = T_{Drive}\omega \quad (83)$$

The scroll efficiency and the overall system thermal efficiency are defined as

$$\eta_{scroll} = \frac{P_{sha}}{P_{WF}} \quad (84)$$

$$\eta_{overall} = \frac{P_{load}}{P_{WF}} \quad (85)$$

where P_{load} is electrical power output by generator.

4. Simulation process and results

The geometric and mathematical models developed in Sections 2 and 3 are programmed using Matlab. Fig. 11 depicts the procedure to conduct the simulation as described in detail as follows.

(1) Input all scroll geometric parameters, the inlet working fluid pressure and temperature, the back pressure and temperature. The procedure starts at orbiting angle $\theta = 0°$ and $\omega = 0$ rad s^{-1}. The initial pressure and temperature in each chamber are assumed to be the same as back pressure and temperature. The volume of each chamber is calculated on the basis of scroll geometry with the orbiting angle. The working fluid density and mass are calculated according to

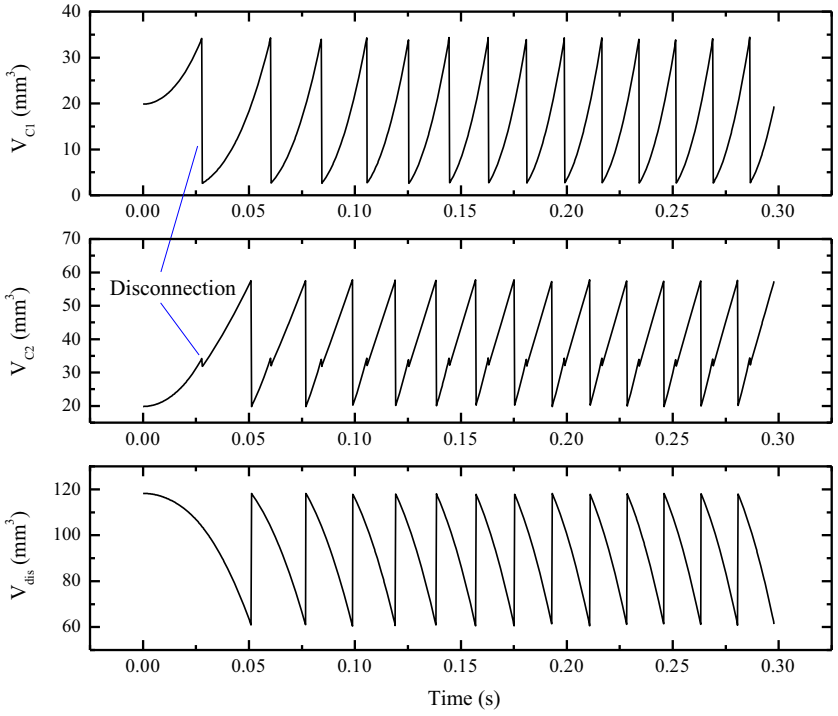

Fig. 12. Chamber volume variation, P_{in} = 3.0 bar, R_{load} = 20.0 Ω.

the pressure and temperature. A maximum time interval and a maximum angle interval are pre-set to start the simulation.

(2) Based on previous working fluid pressures in each chamber, the motion equation is called to calculate the drive torques, rotational speed of the scroll, the angular velocity, and the orbiting angle. The time interval should be adjusted if the increment of the calculated orbiting angle turns out to be larger than expected.

(3) The valve model is called to calculate the mass flow rate at the inlet of the expander and the mass flow rate that exits the discharge chamber, which are unnecessary the same in

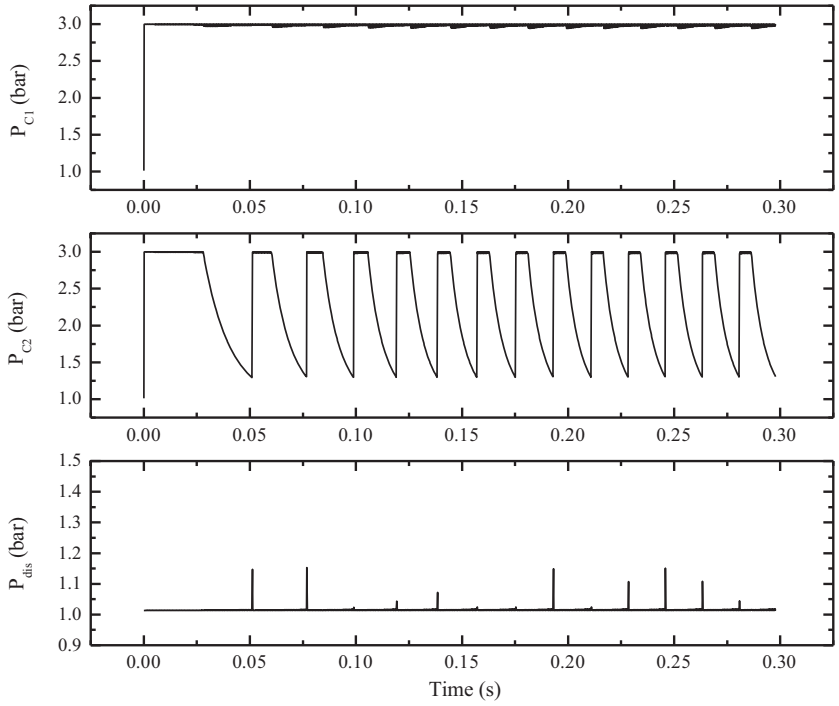

Fig. 13. Chamber pressure variation, P_{in} = 3.0 bar, R_{load} = 20.0 Ω.

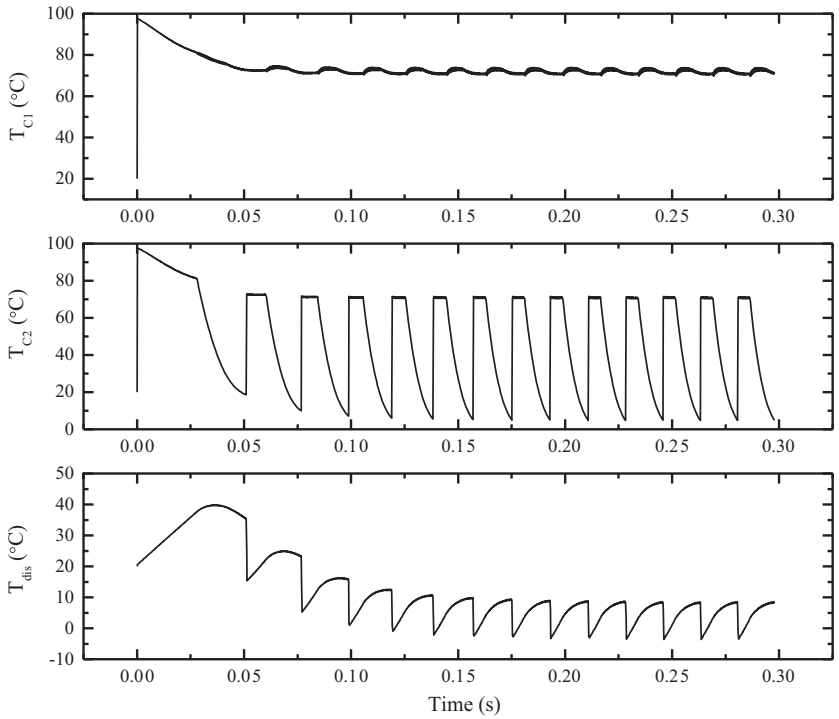

Fig. 14. Chamber temperature variation, P_{in} = 3.0 bar, R_{load} = 20.0 Ω.

the dynamic model. The leakage model is used to calculate the internal leakage between chambers. The mass amount of working fluid inside each chamber must be ensured to be larger than zero.

(4) A new volume value of each chamber is calculated based on the scroll geometry using the new orbiting angle obtained in step 2.

(5) The heat transfer equation is called to calculate the mean heat transfer rate into each chamber from adjacent chambers and the ambient.

(6) A guess of pressure value in each chamber is given as an initiate value to solve the energy balance equation, the new states of the working fluid are then obtained. Based on the comparison between the initial guess value and the new calculated one, an adjusted pressure value is given to repeat the calculation. Such an iteration process continues until the convergence is achieved between the latest input pressure value and the lastly obtained value.

(7) Steps 2–6 are repeated at the given time interval until reaching the assumed operation time.

The simulation results based on the scroll and generator parameters and the working conditions presented in Table 2 are shown in Figs. 12–15. At the very beginning, $\theta = 0°$, there is a merged chamber by chamber 1 and 2 due to the scroll modification. Once the scroll starts rotating, the volume of this merged chamber increases. The disconnection occurs at θ_{disc} as the merged chamber splits into a small chamber, chamber 1, and a large chamber, chamber 2. Thereafter, these two chambers go on expansion until $\theta = 2\pi$. In the meantime, the discharge chamber volume reduces since chamber 1 and 2 all expands and the total expander volume remains constant. Fig. 13 shows the chamber pressure variation. The chamber 1 pressure is slightly lower than the inlet pressure because of the pressure drop of the inlet working fluid when it passes through the intake valve before reaching chamber 1. After disconnection between the chamber 1 and 2, the chamber 2 pressure reduces as the chamber volume increases, but at the end of each cycle it is still higher than the back pressure, that indicates the working fluid is not over-expanded. The discharge chamber is connected to the atmosphere in the current study case, hence the discharge pressure equals to the atmospheric pressure for most of the time; however, the discharge pressure elevates slightly at the moment of $\theta = 2\pi$ because the chamber 2 with higher pressure working fluid merges with the discharge chamber. The chamber temperature variation is shown in Fig. 14. As the expander starts rotating, the temperature of the merged chamber by chamber 1 and 2 increases drastically due to the feed-in fluid and the sudden pressure raise. Thereafter, the chamber 1 temperature varies little due to the continuous supply of the inlet working fluid; however, the chamber 1 temperature is found lower than that of the inlet working fluid because of the slight pressure reduction after the fluid passing through the valve and the ongoing expansion. The chamber 2 temperature drops rapidly after the disconnection because of the relatively violent expansion. The discharge chamber temperature increases during each rotational cycle since the working fluid experiences compression in this chamber; at the moment of $\theta = 2\pi$, the discharge chamber temperature drops as shown in Fig. 14, which is the result of the mixing with the lower temperature working fluid from the opened chamber 2 and the venting to the ambient at the same time.

Fig. 15 shows the variations of rotational speed and the generated current with different inlet pressure of working fluid and different electric load resistance. Higher inlet pressure leads to higher scroll rotational speed since more tangent force is produced by larger pressure difference, as shown in Fig. 15(a), meanwhile the corresponding generated current is larger as well, as

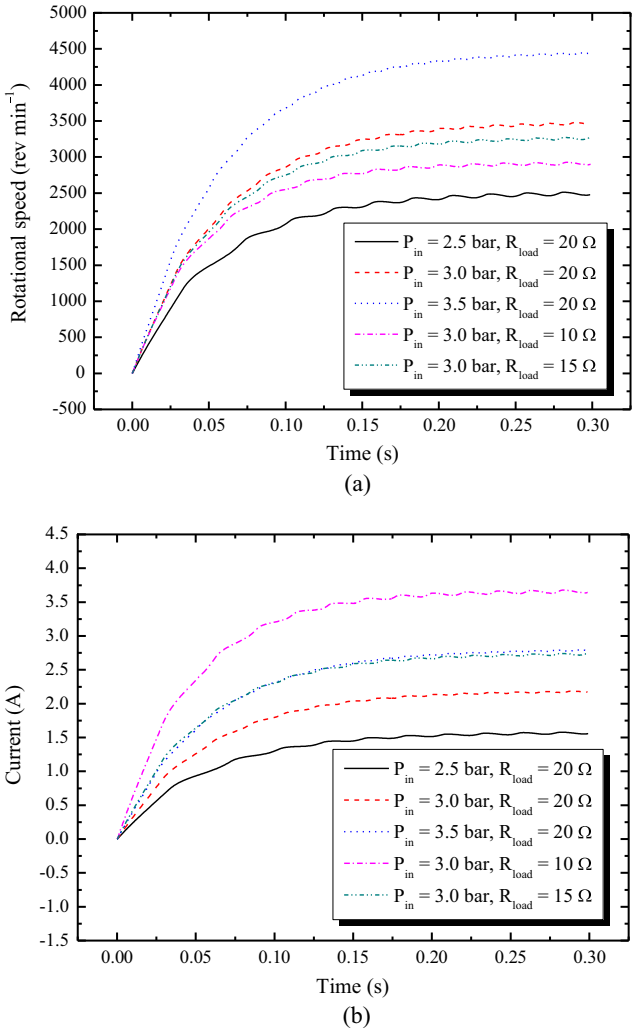

Fig. 15. Simulated performance of scroll expander – generator system with different inlet pressure of working fluid and electric load resistance, (a) rotational speed; (b) generated current.

shown in Fig. 15(b). Another influence factor for the rotational speed and the current is the electric load resistance. Apparently, the higher the load resistance is, the lower the current is; thereby the required electromechanical torque is smaller as can be explained by Eq. (67). That results in more torque to conquer the mechanical friction for higher rotational speed. The overall efficiency of the scroll expander – generator system as calculated by Eq. (85) is presented in Fig. 16. The inlet pressure of the working fluid hardly affects the efficiency if the load resistance is constant. As the inlet pressure increases, the produced mechanical energy, the kinetic energy to maintain the rotation of the scroll and generator, the mechanical friction loss, and the electromechanical energy all generally increase proportionally, hence the overall efficiency nearly remains the same. However, in practice, the mechanical friction loss is not linearly varying with the rotational speed as being assumed in the present simulation, the friction coefficient may increase with the increasing pressure difference, then the overall energy efficiency varies non-linearly with the inlet pressure. Further study about the relationship between mechanical friction loss and pressure difference can be referred to literatures [31–33]. Additionally, the reduction of the load resistance leads to higher overall efficiency. As the foregoing discussion, lower load resistance leads to higher generated current but lower rotational speed, then both the consumed kinetic energy and mechanical

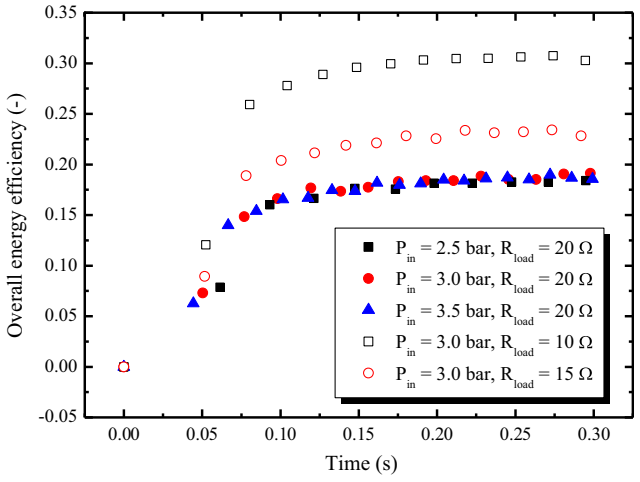

Fig. 16. Overall energy efficiency of scroll expander – generator system with different inlet pressure of working fluid and electric load resistance.

friction loss are smaller, consequently, the overall energy efficiency is higher because the total produced mechanical energy changes little in response to the reduced load resistance.

5. Test bench and experimental validations

Experimental tests were carried out to validate the present models and simulation, the test bench is schematically shown in Fig. 17. The tested oil-free scroll expander (E15H22N4.25, manufactured by Air Squared Inc.©) has a nominal output of 1.0 kW, an expansion ratio of 3.5:1 and a displacement of 12 mm^3 rev^{-1}. Compressed air was used as the working fluid and was supplied by an air compressor with a storage tank attached. The exhausted air was discharged to the ambient directly. An AC generator (Voltmaster AB30L, supplied by Wanco Inc.©) was coupled coaxially with the expander through magnetic coupling. An electric load bank was used with the resistance around 82.0 Ω.

The inlet and outlet temperature and pressure of the expander were measured by Pt100 sensors (accuracy 0.01 °C) and electric pressure transducer (0–25 bar, accuracy ±0.1%). The inlet air pressure was adjusted by a manual valve while the inlet temperature was at the ambient temperature. A vortex flow meter (accuracy ±1%) was installed at the inlet of the expander to record the volume flow rate of the compressed air. A non-contact pocket laser tachometer (HHT12, Omega©, accuracy 0.01%) was used to measure the rotational speed of the expander. The generated electrical voltage, current and power were measured by a power meter (ZW2613, Qingzhi©, accuracy 0.5%).

To acquire the geometric parameters of the scroll, the expander was disassembled after testing as the internal view is shown in Fig. 18. The scroll expander had four pairs of expansion chamber. The scroll thickness, height and pitch as well as the scroll base plate dimensions were measured directly. Other parameters, including basic circle radius, initial involute angle and orbiting radius were derived from Eqs. (12)–(14). The mass of the orbiting scroll could be calculated by its volume and material density, thereafter the inertia moment of the orbiting scroll was calculated

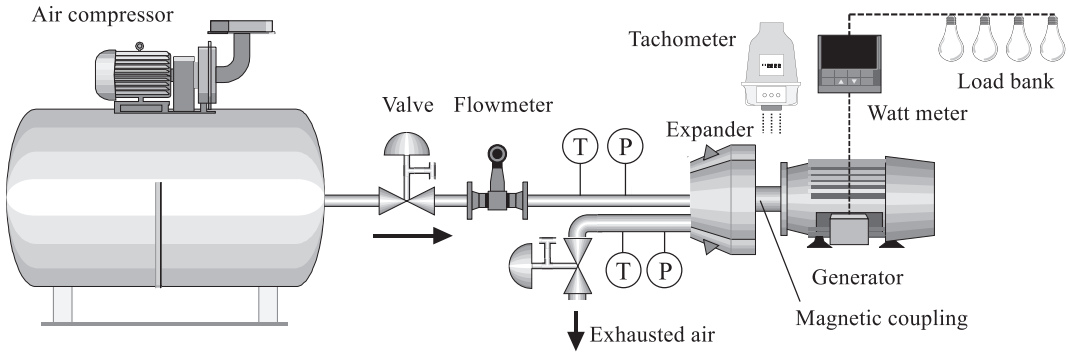

Fig. 17. Schematic diagram of the scroll expander test bench.

Fig. 18. Photos of the disassembled scroll expander after testing.

Table 3
Geometric parameters of the tested scroll expander.

Variables	Values
a	2.37 mm[a]
α	49.25°[a]
t_s	4.08 mm[b]
Pit	14.91 mm[b]
h_s	22.40 mm[b]
R_{or}	3.38 mm[a]
N_C	4[b]
J_{orb}	1.24×10^{-5} kg m^2[a]
δ_r, δ_f	0.01 mm[c]
f_r, f_f	0.9[c]

[a] These values were calculated by present scroll geometric models.
[b] These values were measured directly.
[c] These values were estimated based on literature [18].

based on Eq. (64). The tested expander has no Oldham ring, the self-rotation of the orbiting scroll was prevented by three rotatable connector at the corner of the triangular scroll base plate. All the parameters of the scroll expander are presented in Table 3.

The used AC generator has a rated power output of 2.4 kW, rated amps of 10 A, rated volts of 240 V and maximum rotational speed of 3000 rev min^{-1}. The inertia moment of the generator shaft and armature is given by the manufacturer as 0.0057 kg m^2. To make the scroll expander modelling easier and more accurate, a correlation between rotational speed and output electricity power was developed for the generator based on the experimental results so that it could be used in the simulation to calculate the electric current and the electromechanical torque and so on.

It should be noted that the overall dynamic friction coefficient of the scroll and generator, f_{SG}, is still unknown at this stage. Therefore, the experimental results should be analysed to determine this value, viz. the value of f_{SG} in the model was trialled and adjusted to achieve the best agreement between the measured and simulated results. The experimental data and simulated results in terms of rotational speed and output power is compared in Fig. 19(a). It was found that f_{SG} was not constant but increased from 0.0019 N m s to 0.0064 N m s as the inlet pressure of the working fluid increasing from about 3.0 bar to 11.0 bar, as shown in Fig. 19(b).

Experimental data reported by other researchers [18,20] have also been used to validate the present models and simulation method. Using air as the working fluid to evaluate the scroll expander performance, the measured output current and the rotational speed reported in literature [18] and the simulated results using the present models in this work, are compared in Fig. 20. The numerical model of the DC generator was integrated in the simulation. All the parameters of the employed scroll expander and DC generator as well as the working conditions are presented in Table 4. Since the inlet working fluid pressure was in a small range of 2.0–2.55 bar, the value of f_{SG} was considered as constant. Eventually, in order to achieve the best agreement between the measured and simulated results, the value of f_{SG} was determined as 0.0034 N m s. Another experimental study [20] that used compressed air as the working fluid to drive a scroll expander, has the scroll geometry parameters and working conditions listed in Table 5, but no information about the generator was provided by the work [20]. A correlation of electromechanical torque against the rotational speed for the used generator based on the same testing setup was reported by the same researchers in another work [21], which was used in present simulation. The feed-in compressed air had a constant pressure at 3.7 bar, hence the value of f_{SG} was reasonably considered as constant. The best agreement between the measured values of output power and mass flow rate [20] and the simulated results using the present models are shown

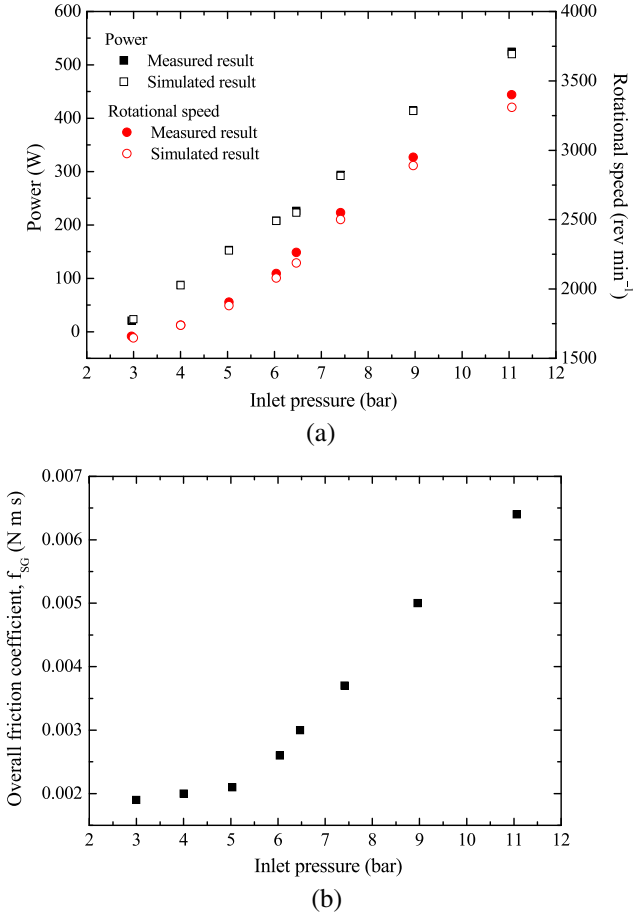

Fig. 19. Validation of the modelling and simulation by present experimental results, (a) comparison between the measured and simulated output power and rotational speed; (b) the obtained overall dynamic friction coefficient.

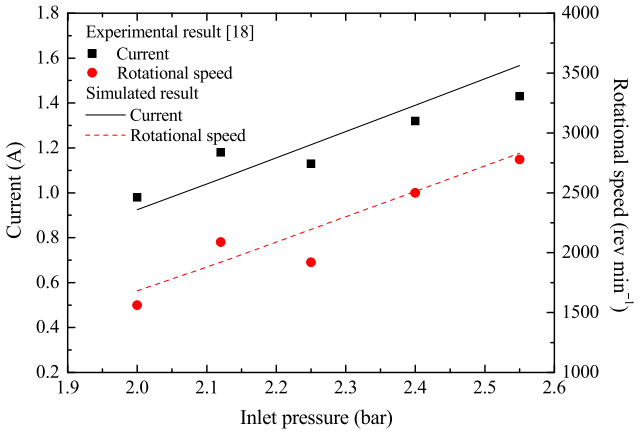

Fig. 20. Comparison between the experimental [18] and simulated results of output current and rotational speed.

in Fig. 21, with the determined f_{SG} value of 0.003 N m s, which is lower than that determined based on experimental results reported by literature [18] despite of its larger pressure difference. Therefore, it can be concluded that f_{SG} is dominated not only by pressure difference imposing on the expander but also the specification of the employed expander – generator system.

Table 4
Parameters used in the simulation of experimental test reported by Wang et al. [18].

Scroll parameters	
a	3.35 mm[a]
α	41.05°[a]
t_s	4.8 mm[b]
Pit	21.05 mm[a]
h_s	30.7 mm[b]
R_{or}	5.8 mm[b]
N_C	2[b]
J_{orb}	9.3×10^{-6} kg m^2[a]
J_{Old}	1.35×10^{-6} kg m^2[a]
δ_r, δ_f	0.015 mm, 0.01 mm[b]
f_r, f_f	0.9[b]
Generator parameters (DC generator)	
$J_{sha} + J_{arm}$	2.2×10^{-4} kg m^2[c]
R_a	0.5 Ω[b]
R_{load}	22.2 Ω[b]
K_e, K_t	0.12 N m A^{-1}[b]
L_a	0.00061 H[b]
f_{SG}	0.0034 N m s[d]
Valve parameters	
C_v	36[e]
x_T	0.86[e]
Working conditions	
Working fluid	Air[b]
P_{in}	2.0–2.55 bar[b]
T_{in}	26.85 °C[b]
P_b	1.013 bar[b]
T_b	26.85 °C[b]

[a] These values were calculated by present scroll geometric models.
[b] These values were given by the original literature [18].
[c] These value was supplied by the manufacturer.
[d] This value was determined by present simulation.
[e] These values were estimated based on literature [29].

Table 5
Parameters used in the simulation of experimental test reported by Liu et al. [20].

Scroll parameters	
a	3.66 mm[a]
α	36°[a]
t_s	4.6 mm[b]
Pit	23.0 mm[b]
h_s	40 mm[a]
R_{or}	6.9 mm[a]
N_C	3[a]
J_{orb}	3.38×10^{-5} kg m^2[b]
J_{Old}	2.93×10^{-6} kg m^2[b]
δ_r, δ_f	0.02 mm[d]
f_r, f_f	0.9[b]
Generator parameters (AC generator)	
$J_{sha} + J_{arm}$	7.45×10^{-4} kg m^2[b]
R_{load}	20–80 Ω[d]
f_{SG}	0.003 N m s[d]
Valve parameters	
C_v	34[c]
x_T	0.86[c]
Working conditions	
Working fluid	Air[a]
P_{in}	3.7 bar[a]
T_{in}	19.0 °C[a]
P_b	1.013 bar[a]
T_b	15.2 °C[a]

[a] These values were given by the original literature [18].
[b] These values were calculated by present scroll geometric models.
[c] These values were estimated based on literature [29].
[d] These values were determined by present simulation.

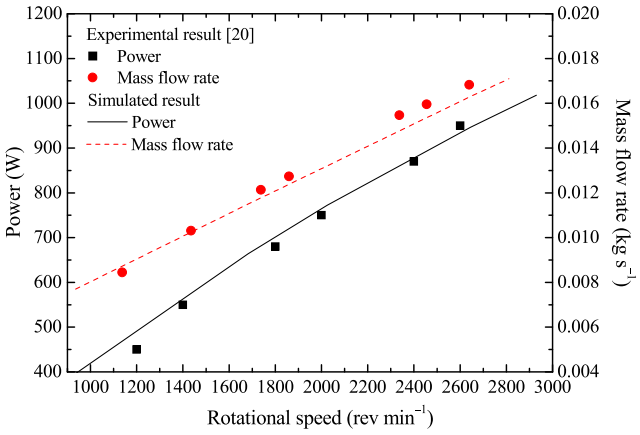

Fig. 21. Comparison between the experimental [20] and simulated results of output power and mass flow rate.

6. Conclusions

This work presented in detail a more generic model and simulation method of scroll expander used for small scale power generation system, which was sufficiently validated by experimental results, either conducted by the authors or previously reported by other researchers. As an indispensable but rarely reported value, the overall dynamic friction coefficient of the scroll expander – generator system, f_{SG}, was studied and highlighted in the present model, which can be determined by the experiments for a specific expander – generator system without cumbersome relation formulae and detailed information collection. As the inlet pressure of the working fluid increases from about 3.0 bar to 11.0 bar in the experiment carried out in this work, the determined f_{SG} increased from about 0.0019 N m s to 0.0064 N m s, which is reasonable in practice since larger pressure difference resulted in larger friction force. When the difference between the inlet pressure of the working fluid and the back pressure was constant or varying within a small range, the f_{SG} can be treated as a constant value despite of the variation of the load resistance. The accurate f_{SG} value of each expander – generator system should be determined by practical tests for precise modelling, once the f_{SG} is obtained by a few tests, the simulation can be implemented to predict the system performance over a wider range of operational conditions.

Acknowledgement

The authors gratefully acknowledge the support from the IAA project (Impact Acceleration Account) (EP/K503885/1) and IDRIST project (EP/M008088/1), funded by the Engineering and Physical Science Research Council of UK. Data supporting this publication is openly available under an 'Open Data Commons Open Database License'. Additional metadata are available at: http://dx.doi.org/10.17634/148532-4. Please contact Newcastle Research Data Service at rdm@ncl.ac.uk for access instructions.

Appendix A. Modification area and volume by circular cutter

Fig. A1 is given to aid the calculation of this modification area by geometric method. The following steps are established to gain the modification area. Firstly, the entire area is divided into two separate areas

$$S_{mc} = A_{MHDF} + A_{DFPG} \quad (A1)$$

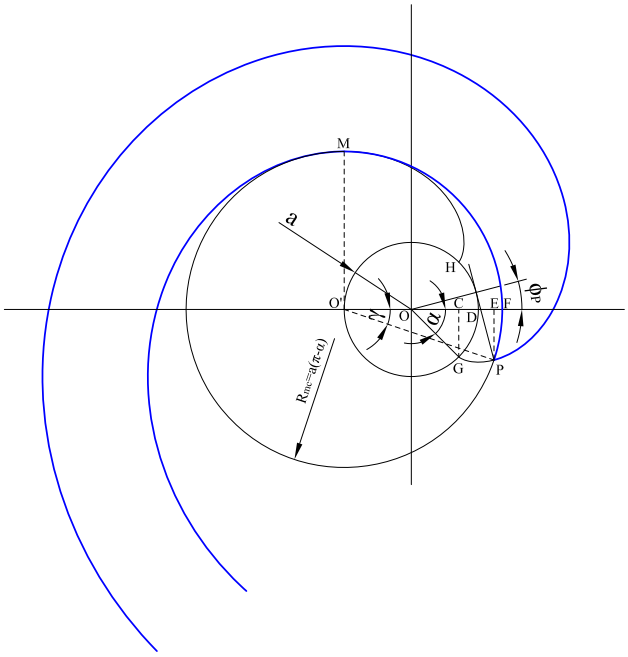

Fig. A1. Area calculation of the modified chamber 1 by circular cutter.

The area of MHDF is calculated by the following equation

$$\begin{aligned} A_{\mathrm{MHDF}} &= \pi R_{\mathrm{mc}}^2/4 - \pi a^2/2 - f_{\mathrm{s}}(\mathrm{F(M)}) \\ &= \pi a^2(\pi-\alpha)^2/4 - \pi a^2/2 - \frac{a^2(\pi-\alpha)^3}{6} \end{aligned} \tag{A2}$$

The area of DFPG can be divided into small pieces

$$A_{\mathrm{DFPG}} = A_{\mathrm{DEPG}} + A_{\mathrm{EFP}} = A_{\mathrm{CEPG}} - A_{\mathrm{CDG}} + A_{\mathrm{EFP}} \tag{A3}$$

where each individual area is calculated by following equations

$$A_{\mathrm{CDG}} = A_{\mathrm{ODG}} - A_{\mathrm{OCG}} = \frac{\alpha a^2}{2} - \frac{a^2 \sin\alpha\cos\alpha}{2} \tag{A4}$$

$$A_{\mathrm{EFP}} = A_{\mathrm{O'FP}} - A_{\mathrm{O'EP}} = \frac{\gamma R_{\mathrm{mc}}^2}{2} - \frac{R_{\mathrm{mc}}^2 \sin\gamma\cos\gamma}{2} \tag{A5}$$

$$\sin\gamma = \frac{|y_{\mathrm{P}}|}{R_{\mathrm{mc}}} = \frac{|a(\sin\phi_{\mathrm{P}} - (\phi_{\mathrm{P}}+\alpha)\cos\phi_{\mathrm{P}})|}{R_{\mathrm{mc}}} \tag{A6}$$

$$\begin{aligned} A_{\mathrm{CEPG}} &= -\int_{x_{\mathrm{G}}}^{x_{\mathrm{P}}} y_{\mathrm{o}}\,\mathrm{d}x_{\mathrm{o}} = -\int_{-\alpha}^{\phi_{\mathrm{P}}} a(\sin\phi - (\phi+\alpha)\cos\phi)\mathrm{d} \\ &\quad \times (a(\cos\phi + (\phi+\alpha)\sin\phi)) \\ &= -a^2\int_{-\alpha}^{\phi_{\mathrm{P}}} (\phi+\alpha)\cos\phi(\sin\phi - (\phi+\alpha)\cos\phi)\mathrm{d}\phi \\ &= a^2\left(\frac{\alpha^2+\phi_{\mathrm{P}}^2+2\alpha\phi_{\mathrm{P}}-1}{4}\sin(2\phi_{\mathrm{P}}) + \frac{\alpha+\phi_{\mathrm{P}}}{2}\cos(2\phi_{\mathrm{P}})\right. \\ &\quad \left. - \frac{\sin(2\alpha)}{4} + \frac{(\alpha+\phi_{\mathrm{P}})^3}{6}\right) \end{aligned} \tag{A7}$$

The total modification volume is then calculated based on the modification area and the scroll height using the following equation

$$V_{\mathrm{mc}} = 2h_{\mathrm{s}}S_{\mathrm{mc}} \tag{A8}$$

Appendix B. Modification area and volume by PMP method

The geometric method to calculate the modification area by using PMP method is with the help of Fig. 5(b). The area of FO_2OO_1-GF is calculated firstly by considering the identical congruence of triangles ΔODO_1 and ΔOEO_2.

$$\begin{aligned} A_{\mathrm{FO_2OO_1GF}} &= f_{\mathrm{s}}(\mathrm{F'(F)}) - f_{\mathrm{s}}(\mathrm{F'(A)}) + \frac{\pi a^2}{2} - A_{\mathrm{O_1AG}} \\ &= \frac{a^2}{6}\left[(\phi_{\mathrm{A}}+\pi+\alpha)^3 - (\phi_{\mathrm{A}}+\alpha)^3\right] + \frac{\pi a^2}{2} - A_{\mathrm{O_1AG}} \end{aligned} \tag{A9}$$

So the modified scroll wrap ending at points F and B has the projected area of

$$\begin{aligned} A_{\mathrm{scroll-FB}} &= A_{\mathrm{FO_2OO_1GF}} - A_{\mathrm{O_2BC}} + A_{\mathrm{O_1AC}} + A_{\mathrm{O_1AG}} \\ &= \frac{a^2}{6}\left[(\phi_{\mathrm{A}}+\pi+\alpha)^3 - (\phi_{\mathrm{A}}+\alpha)^3\right] + \frac{\pi a^2}{2} - \frac{\lambda}{2}R_2^2 + \frac{\lambda}{2}R_1^2 \end{aligned} \tag{A10}$$

The increased expansion area caused by the modification is then

$$\begin{aligned} S_{\mathrm{mp}} &= f_{\mathrm{s}}(\mathrm{F'(F)}) - f_{\mathrm{s}}(\mathrm{F(B)}) - A_{\mathrm{scroll-FB}} \\ &= \frac{a^2}{6}\left[(\phi_{\mathrm{A}}+\pi+\alpha)^3 - (\phi_{\mathrm{A}}+\pi-\alpha)^3\right] \\ &\quad - \left(\frac{a^2}{6}\left[(\phi_{\mathrm{A}}+\pi+\alpha)^3 - (\phi_{\mathrm{A}}+\alpha)^3\right] + \frac{\pi a^2}{2} - \frac{\lambda}{2}R_2^2 + \frac{\lambda}{2}R_1^2\right) \\ &= \frac{a^2}{6}\left[(\phi_{\mathrm{A}}+\alpha)^3 - (\phi_{\mathrm{A}}+\pi-\alpha)^3\right] - \frac{\pi a^2}{2} + \frac{\lambda}{2}R_2^2 - \frac{\lambda}{2}R_1^2 \end{aligned} \tag{A11}$$

The total increased volume caused by modifying both the orbiting and fixed scroll is obtained as the following equation.

$$V_{\mathrm{mp}} = 2h_{\mathrm{s}}S_{\mathrm{mp}} \tag{A12}$$

Appendix C. Volume variation of chamber 1 and chamber 2 by using PMP modification

If the scroll is modified by PMP, the area and volume calculation can be specified to three different scenarios as illustrated in Fig. A2. When the orbiting angle θ is smaller than γ, chamber 1 and 2 are connected, in this case their volume can be calculated by the following equation

$$V_{\mathrm{C1\text{-}mp}} = V_{\mathrm{C2\text{-}mp}} = V_{\mathrm{C1}} + V_{\mathrm{C2}} + V_{\mathrm{mp}} \quad \theta < \gamma \tag{A13}$$

When $\theta = \gamma$, the two scrolls are meshed at the connection point of two modification circular arcs as shown in Fig. A2(a). When θ value is between γ and $(\gamma + \lambda)$, the modification arcs are shared by the disconnected chamber 1 and 2 as shown in Fig. A2(b). The area of chamber 1, which is the enclosed area of ABCDEFA is calculated by

$$\begin{aligned} A_{\mathrm{ABCDEFA}} &= 2(A_{\mathrm{AO_{2\_f}EFA}} - A_{\mathrm{AO_{1\_o}BA}}) - A_{\mathrm{O_{1\_o}O_{2\_o}O_{1\_f}O_{2\_f}O_{1\_o}}} \\ &= 2\frac{\theta-\gamma}{2}\left(R_2^2 - R_1^2\right) - (R_2-R_1)(R_2+R_1)\sin(\theta-\gamma) \\ &= (R_2^2 - R_1^2)(\theta - \gamma - \sin(\theta-\gamma)) \end{aligned} \tag{A14}$$

Hence, the volume of chamber 1 and 2 can be obtained by the following equations.

$$V_{\mathrm{C1\text{-}mp}} = h_{\mathrm{s}}\left(R_2^2 - R_1^2\right)(\theta - \gamma - \sin(\theta-\gamma)) \quad \gamma \leqslant \theta < \gamma + \lambda \tag{A15}$$

$$V_{\mathrm{C2\text{-}mp}} = V_{\mathrm{C1}} + V_{\mathrm{C2}} + V_{\mathrm{mp}} - V_{\mathrm{C1\text{-}mp}} \quad \gamma \leqslant \theta < \gamma + \lambda \tag{A16}$$

When $\theta \geqslant \gamma + \lambda$, as shown in Fig. A2(c), the modification arcs are only involved in the enclosure of chamber 1, therefore the volume values become as follows.

$$V_{\mathrm{C1\text{-}mp}} = V_{\mathrm{C1}} + V_{\mathrm{mp}} \quad \theta \geqslant \gamma + \lambda \tag{A17}$$

$$V_{\mathrm{C2\text{-}mp}} = V_{\mathrm{C2}} \quad \theta \geqslant \gamma + \lambda \tag{A18}$$

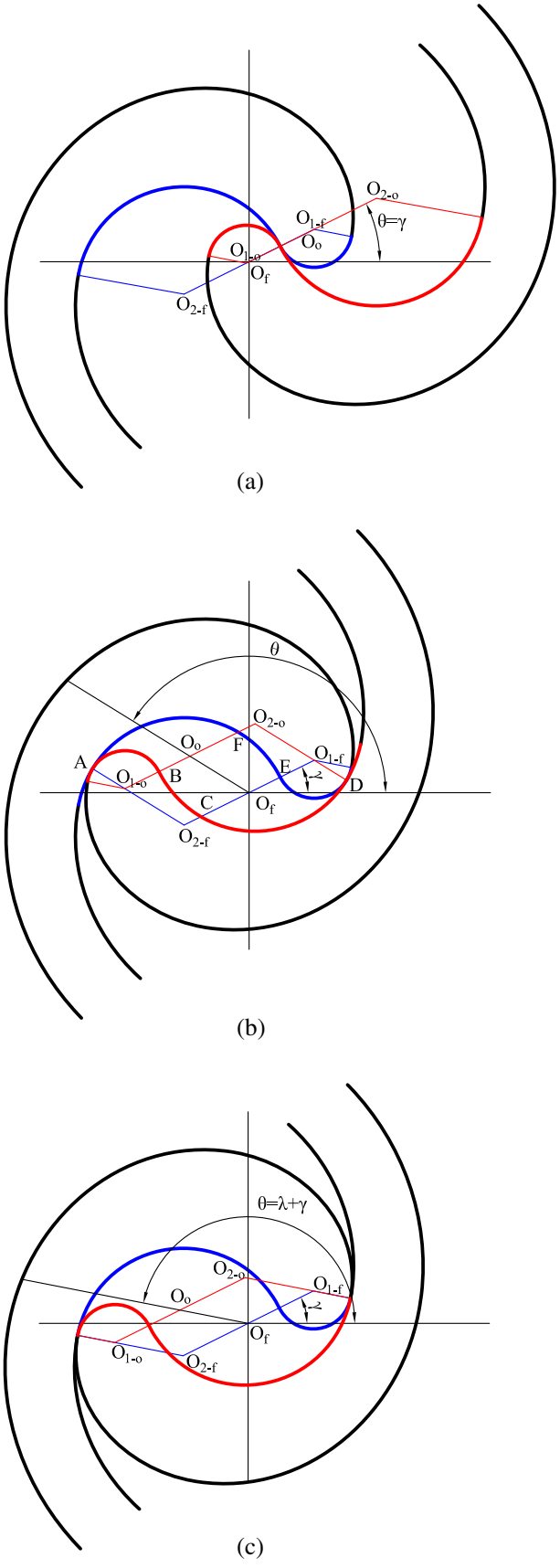

Fig. A2. Area calculation of the modified chamber 1 by PMP, (a) $\theta = \gamma$, (b) $\gamma \leq \theta < \lambda + \gamma$, (c) $\theta = \lambda + \gamma$.

References

[1] Qiu G, Liu H, Riffat S. Expanders for micro-CHP system with organic Rankine cycle. Appl Therm Eng 2011;31:3301–7.
[2] Bao J, Zhao L. A review of working fluid and expander selections for organic Rankine cycle. Renew Sustain Energy Rev 2013;24:325–42.
[3] Song P, Wei M, Shi L, Danish SN, Ma C. A review of scroll expanders for organic Rankine cycle systems. Appl Therm Eng 2015;75:54–64.
[4] Lemort V, Declaye S, Quoilin S. Experimental characterization of a hermetic scroll expander for use in a micro-scale Rankine cycle. Proc IMechE, Part A: J Power Energy 2012;226:126–36.
[5] Bracco R, Clemente S, Micheli D, Reini M. Experimental tests and modelization of a domestic-scale ORC (organic Rankine cycle). Energy 2013;58:107–16.
[6] Lemort V, Quoilin S, Cuevas C, Lebrun J. Testing and modeling a scroll expander integrated into an organic Rankine cycle. Appl Therm Eng 2009;29:3094–102.
[7] Quoilin S, Lemort V, Lebrun J. Experimental study and modeling of an organic Rankine cycle using scroll expander. Appl Energy 2010;87:1260–8.
[8] Declaye S, Quoilin S, Guillaume L, Lemort V. Experimental study on an open-drive scroll expander integrated into an ORC (organic Rankine cycle) system with R245fa as working fluid. Energy 2013;55:173–83.
[9] Chang JC, Huang TC, He YL, Zhang W. Experimental study on low-temperature organic Rankine cycle utilizing scroll type expander. Appl Energy 2015;155:150–9.
[10] Galloni E, Fontana G, Staccone S. Design and experimental analysis of a mini ORC (organic Rankine cycle) power plant based on R245fa working fluid. Energy 2015;90:768–75.
[11] Mendoza LC, Navarro-Esbri J, Bruno JC, Lemort V, Coronas A. Characterization and modelling of a scroll expander with air and ammonia as working fluid. Appl Therm Eng 2014;70:630–40.
[12] Iglesias A, Favrat D. Innovative isothermal oil-free co-rotating scroll compressor-expander for energy storage with first expander tests. Energy Convers Manage 2014;85:565–72.
[13] Yang X, Pan J, Wang J, Sun J. Simulation and experimental research on energy conversion efficiency of scroll expander for micro-compressed air energy storage system. Int J Energy Res 2014;38:884–95.
[14] Gao X, Li L, Zhao Y, Shu P, Shen J. Research on a scroll expander used for recovering work in a fuel cell. Int J Thermodyn 2004;7:1–8.
[15] Bao HS, Wang YD, Charalambous C, Lu ZS, Wang LW, Wang RZ, et al. Chemisorption cooling and electric power cogeneration system driven by low grade heat. Energy 2014;72:590–8.
[16] Jiang L, Wang LW, Liu CZ, Wang RZ. Experimental study on a resorption system for power and refrigeration cogeneration. Energy 2016;97:182–90.
[17] Wang J, Yang L, Luo X, Mangan S, Derby JW. Mathematical modeling study of scroll air motors and energy efficiency analysis-Part I. IEEE/ASME Trans Mechatron 2011;16:112–21.
[18] Wang J, Luo X, Yang L, Shpanin LM, Jia N, Mangan S, et al. Mathematical modeling study of scroll air motors and energy efficiency analysis-Part II. IEEE/ASME Trans Mechatron 2011;16:122–32.
[19] Luo X, Wang J, Sun H, Derby JW, Mangan SJ. Study of a new strategy for pneumatic actuator system energy efficiency improvement via the scroll expander technology. IEEE/ASME Trans Mechatron 2013;18:1508–18.
[20] Liu G, Zhao Y, Li L, Shu P. Simulation and experiment research on wide ranging working process of scroll expander driven by compressed air. Appl Therm Eng 2010;30:2073–9.
[21] Liu G, Zhang Y, Yang Q, Wang L, Tang B, Li L. Theoretical and experimental research on scroll expander used in small-scale organic Rankine system. J Process Mech Eng 2015;229:25–35.
[22] Kim HJ, Ahn JM, Park I, Rha PC. Scroll expander for power generation from a low-grade steam source. Proc IMechE, Part A: J Power Energy 2007;221:705–12.
[23] Giuffrida A. Modelling the performance of a scroll expander for small organic Rankine cycles when changing the working fluid. Appl Therm Eng 2014;70:1040–9.
[24] Chang JC, Chang CW, Hung TC, Lin JR, Huang KC. Experimental study and CFD approach for scroll type expander used in low-temperature organic Rankine cycle. Appl Therm Eng 2014;73:1444–52.
[25] Song P, Wei M, Liu Z, Zhao B. Effects of suction port arrangements on a scroll expander for a small scale ORC system based on CFD approach. Appl Energy 2015;150:274–85.
[26] Lee YR, Wu WF. On the profile design of a scroll compressor. Int J Refrig 1995;18:308–17.
[27] Bell I, Groll EA, Braun JE, King G. Update on scroll compressor chamber geometry. In: International compressor engineering conference at Purdue. 1489.
[28] Liptak BG. Process control and optimization. Instrument engineers' handbook. Chapter 6 Control valve selection and sizing, 4th ed., vol. 2. CRC Press; 2005.
[29] Emerson. Control valve handbook. Fisher Controls International LLC; 2005.
[30] Chen Y, Halm NP, Groll EA, Braun JE. Mathematical modeling of scroll compressors-Part I: compression process modeling. Int J Refrig 2002;25:731–50.
[31] Liu Y, Huang C, Chang Y. Design optimization of scroll compressor applied for frictional losses evaluation. Int J Refrig 2010;33:615–24.
[32] Ishii N, Fukushima M, Sawai K, Sano K, Imaichi K. Dynamic behaviour of a scroll compressor (dynamic analysis). JSME Int J 1988;31:58–67.

[33] Ishii N, Yamamoto S, Sano K, Sawai K, Hiwata A, Nakamoto T, et al. Efficiency simulations of a compact CO_2 scroll compressor and its comparison with same cooling capacity R410A scroll compressor. In: Proceedings of the international compressor engineering conference at Purdue. C22–2.
[34] Morishita E, Sugihara M, Inaba T, Nakamura T. Scroll compressor analytical model. In: Proceedings of the international compressor engineering conference at Purdue. p. 487–95.
[35] Hayano M, Sakata H, Nagatomo S, Murasaki H. An analysis of losses in scroll compressor. In: Proceedings of the international compressor engineering conference at Purdue. p. 189–97.
[36] Nishiwaki F, Hasegawa H, Ikoma M, Matsuzaki R, Muramatsu S. Mechanical loss reduction at thrust bearing of scroll compressor using R407C. In: Proceedings of international compressor engineering conference at Purdue. p. 263–8.
[37] Okaichi A, Hasegawa H, Nishiwaki F. A study on lubrication characteristics of journal and thrust bearing in scroll compressors. In: Proceedings of international compressor engineering conference at Purdue. C116.
[38] Ishii N, Oku T, Anami K, Fukuda A. Lubrication mechanism at thrust slide-bearing of scroll compressors (experimental study). In: Proceedings of international compressor engineering conference at Purdue. C103.
[39] Yanagisawa T, Fukuta M, Ogi Y, Hikichi T. Performance of an oil-free scroll-type air expander. In: Proceedings of the IMechE conference on compressors and their systems. p. 167–74.
[40] Kenjo T, Nagamori S. Permanent-magnet and brushless DC motors. Oxford: Clarendon Press; 1985.
[41] Krishnan R. Permanent magnet synchronous and brushless DC motor drives. CRC Press; 2009.
[42] Jiang K, Jeong S. Experimental investigation on convective heat transfer mechanism in a scroll compressor. Int J Refrig 2006;29:744–53.